

On asymptotics and resurgent structures of enumerative Gromov–Witten invariants

RICARDO COUSO-SANTAMARÍA, RICARDO SCHIAPPA,
AND RICARDO VAZ

Making use of large-order techniques in asymptotics and resurgent analysis, this work addresses the growth of enumerative Gromov–Witten invariants — in their dependence upon genus and degree of the embedded curve — for several different threefold Calabi–Yau varieties. In particular, while the leading asymptotics of these invariants at large genus or at large degree is exponential, at combined large genus *and* degree it turns out to be factorial. This factorial growth has a resurgent nature, originating via mirror symmetry from the resurgent-transseries description of the B-model free energy. This implies the existence of nonperturbative sectors controlling the asymptotics of the Gromov–Witten invariants, which could themselves have an enumerative-geometry interpretation. The examples addressed include: the resolved conifold; the local surfaces local \mathbb{P}^2 and local $\mathbb{P}^1 \times \mathbb{P}^1$; the local curves and Hurwitz theory; and the compact quintic. All examples suggest very rich interplays between resurgent asymptotics and enumerative problems in algebraic geometry.

1	Introduction	708
2	Setting the stage and main ideas	712
3	An exactly-solvable model: the resolved conifold	724
4	Computational explorations in Calabi–Yau threefolds	730

Key words and phrases: asymptotics, resurgent analysis, enumerative geometry, algebraic geometry, topological strings, Gromov–Witten invariants, Gopakumar–Vafa invariants.

Appendix A	Analysis of the <i>abc</i>-coefficients	767
Appendix B	Large-order enumerative data	770
References		785

1. Introduction

Geometrical-counting problems, albeit many times rather natural and simple to formulate, may lead to remarkably rich and interesting structures. Among these, enumerative invariants play an important classification role within algebraic geometry. For example, counting pseudo-holomorphic curves inside symplectic manifolds gives rise to the famous Gromov–Witten (GW) invariants. These are invariants associated to the symplectic manifold \mathcal{X} , which are rational numbers (implying a “virtual” counting) depending on both genus, g , and degree, d , of the embedded curve. We shall denote them by $N_{g,d}$. The computation of GW invariants is generically hard, becoming simpler when the manifold is Calabi–Yau (CY) where they are generated by the A-model topological-string free energy. This is a long story which goes back to the discovery of mirror symmetry; see, *e.g.*, [1–10] for early references, and, *e.g.*, [11–15] for reviews.

Consider the A-model on a CY \mathcal{X} , in the large-radius phase (valid when the Kähler parameter t is large). The A-model free energy is then given by an asymptotic, genus expansion

$$(1.1) \quad F(\mathcal{X}) \simeq \sum_{g=0}^{+\infty} g_s^{2g-2} F_g(t),$$

where the genus- g contributions to the free energy may be decomposed as [6]

$$(1.2) \quad F_g(t) = \sum_{d>0} N_{g,d} Q^d.$$

The sum over degree d corresponds to a sum over topological sectors as classified by worldsheet instantons (where $Q = e^{-t}$ in units where $\alpha' = 2\pi$). While this explicitly shows how the topological-string free energy is a generating function for the genus g , degree d , enumerative GW invariants of \mathcal{X} , $N_{g,d}$, the two expansions above have rather different properties: while

the fixed-genus (1.2) is a *convergent* series¹, with a non-zero radius of convergence, (1.1) is instead a *divergent* asymptotic series, with zero radius of convergence; see, *e.g.*, [18]. The reason for this is the factorial growth of the genus- g contributions with genus, as $F_g \sim (2g)!$.

From the standpoint of defining the string free energy, the asymptotic nature of the perturbative expansion (1.1) implies that $F(\mathcal{X})$ cannot be properly defined by perturbation theory alone. One way to move forward is to use the theory of resurgence [19]. In this context, the perturbative expansion gets enlarged into a transseries, an object which fully captures all information concerning the observable that it represents, including both perturbative/analytic components (in powers of the string coupling g_s) and nonperturbative/non-analytic components (in powers of the “instanton” factor e^{-1/g_s}). The asymptotic and resurgent nature of the perturbative sequence implies the existence of these instanton-type terms, of which there can be many distinct types and with different strengths. Remarkably, all these seemingly independent perturbative and nonperturbative sectors in the transseries turn out to be related to each other via a tight web of asymptotic resurgence relations. In particular, the leading factorial growth of perturbation theory is a consequence of these asymptotic relations, as is any other subleading growth correcting that factorial term. As a result, one may in fact extract, or decode, nonperturbative information from perturbation theory alone and vice-versa. Moreover, these interrelations have somewhat universal forms, and should be expected to hold across a wide range of different problems.

In recent years resurgence has been applied within² topological string theory [21–35] and its double-scaled limits at special points in moduli space [22, 24, 28, 29, 36–38]. In particular, nonperturbative transseries-solutions to the holomorphic-anomaly equations of the B-model were constructed in [30, 32, 35]. These references further focused on the example of local \mathbb{P}^2 , a non-compact CY threefold, where a very rich nonperturbative structure was uncovered, with diverse instanton actions vying for dominance on the Borel plane as the moduli changed. In our present paper we wish to turn our attention to the A-model instead, and in particular to the enumerative invariants it generates.

¹Convergence was proved at planar level in [16, 17], although there is no general mathematical proof at arbitrary genus. As we shall see later on, our examples in the present paper also strongly support this convergence property.

²For an introduction to the main ideas of resurgent asymptotics, and a very complete list of references concerning many other recent applications of resurgence, we refer the reader to [20].

From the standpoint of computing enumerative invariants, the convergence properties of their generating functions might not seem terribly important at first sight. It is nonetheless the case that these convergence properties will dictate the asymptotic behavior of these invariants, in genus and in degree, and this is one of the main questions we address in the present work. Furthermore, within the A-model the GW invariants are the internal ingredients constructing the string free energies, and it seems reasonable to transfer resurgence questions and properties from the free energies to the invariants themselves. In particular, one natural question is to ask exactly how the GW invariants are responsible for the (known) factorial growth of the free energies they build. For example, the convergence of (1.2) roughly implies that, at fixed genus, the large-degree asymptotics of the GW invariants³ $N_{g,d}$ corresponds at most to a leading exponential growth. On the other hand, the asymptotic nature of (1.1) might seem to imply that, at fixed degree, the large-genus asymptotics of the GW invariants $N_{g,d}$ corresponds instead to a leading factorial growth, giving rise to the factorial growth inside the free energy. But this will turn out *not* to be the case. The fixed degree, large-genus asymptotics of the GW invariants is *not* factorial, and we shall see how the factorial growth of the free energy is more subtly encoded at the level of GW invariants.

Note that there are some important differences between addressing resurgent transseries for the B-model free energy, and investigating resurgent asymptotics of A-model enumerative invariants. In the former case, one deals with an asymptotic *series*, which subsequently gets completed into a transseries by the addition of new, nonperturbative sectors. In the latter case, one deals instead with a two-dimensional array of (rational) *numbers*, labeled by both genus and degree (which is represented schematically in Figure 1). The GW invariants in this array are not directly the coefficients of any series, so the concept of their transseries extension is not well-defined. However, any asymptotic resurgence relations explaining the different growths of the $N_{g,d}$, in particular along directions with factorial growth, should themselves be dictated by nonperturbative content in the free-energy transseries — possibly also with an enumerative-geometry interpretation. This opens the door to the existence of nonperturbative analogues of the GW invariants. With this idea in mind, we wish to make precise the asymptotic growth of GW invariants along particular directions on this array, as depicted in Figure 1:

³We shall use the notation where the boldface character specifies which index (if any) remains fixed.

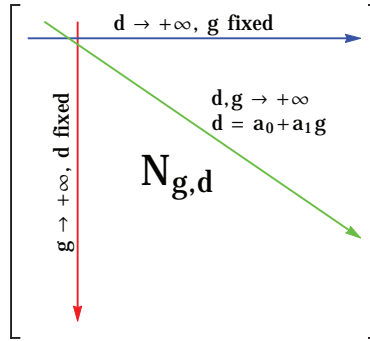


Figure 1. Schematic display of the GW invariants $N_{g,d}$ as a two-dimensional array, with genus and degree representing row and column, respectively. The three arrows are the types of growth that we shall address in this paper: large degree with fixed genus (blue), large genus with fixed degree (red), and combined large degree and genus, with $d = a_0 + a_1 g$ (green).

- **Fixed-genus**, large-degree. Possibly the most “classical” direction previously addressed in the literature, giving rise to leading exponential growth.
- ↓ Large-genus, **fixed-degree**. Less studied, also giving rise to leading exponential growth.
- ↘ Large-genus, large-degree. Not previously addressed in the literature, finally giving rise to the factorial growth characteristic of the free energy.

Asymptotics of GW invariants⁴, with focus on the fixed-genus and large-degree regime, have been previously addressed in [6, 41–43], where leading exponential growth was found. A fixed-degree, large-genus analysis was done

⁴Asymptotics of related enumerative invariants, such as Donaldson–Thomas or Gopakumar–Vafa invariants, and their relevance towards the computation of M-theoretic black hole entropies, have been addressed in [39, 40].

in [44, 45], albeit in a different set-up⁵, also finding leading exponential behavior. To the best of our knowledge, the “enumerative source” of the free-energy factorial growth has never been addressed previously in the literature, and we start filling such gap with our present work. We shall investigate these different asymptotics in several examples, including both compact and non-compact CY threefolds. In particular, our analysis of the exponential growth along horizontal and vertical directions both recovers and generalizes some of the aforementioned previously-known results. The factorial growth is new, and relates to the B-model transseries with its plethora of nonperturbative sectors. Along certain diagonal directions we uncover an universal behavior which is common to geometries in different topological-string universality classes, and which is controlled by the large-radius instanton action. Asymptotic resurgence-like formulae may be written for the “diagonal” growth of GW invariants, with their growth dictated by nonperturbative information encoded in the free-energy transseries. In this sense, one should not wonder about transseries completions of GW invariants, but rather about decoding possibly new “nonperturbative” enumerative invariants, hidden inside the nonperturbative completions to the B-model topological-string transseries [30, 32, 35].

2. Setting the stage and main ideas

Let us formalize the ideas spelled out in our introduction, before addressing an exactly-solvable model (the resolved conifold) in Section 3, and then computationally addressing many different examples in Section 4, including the cases of local \mathbb{P}^2 , a diagonal slice of local $\mathbb{P}^1 \times \mathbb{P}^1$, some local curves, Hurwitz theory, and the quintic compact CY threefold. We begin with general expectations and what sort of structures we wish to unveil, to later materialize in our examples.

Going back to the topological-string asymptotic-series for the free energy (1.1), let us describe it in the B-model as $F^{(0)}(g_s; z, \bar{z})$. Here, the string coupling g_s is also the resurgent variable, and the (0) superscript specifies perturbative. The pair (z, \bar{z}) may be regarded as just external parameters,

⁵References [44–46] address the asymptotics of Weil–Petersson volumes of moduli spaces of algebraic curves, with genus g and n marked punctures (which in some sense corresponds to addressing enumerative invariants of a point). Note that they find some (extra) factorial growth $\sim n!$, but which is associated to the (extra) number of punctures, n . In our context this number is $n = 0$, as GW invariants arise from the free energy.

or interpreted as complex-structure moduli of the underlying CY threefold. The free energy is asymptotic, of Gevrey-1 type (see, *e.g.*, [47]),

$$(2.3) \quad F^{(0)} \simeq \sum_{g=0}^{+\infty} g_s^{2g-2} F_g^{(0)}, \quad F_g^{(0)} \sim \Gamma(2g-1) \text{ as } g \rightarrow +\infty,$$

for generic values of (z, \bar{z}) . Understanding the resurgent properties of $F^{(0)}$ and the role played by the moduli (z, \bar{z}) was the main purpose of [30, 32]. There, it was shown how to look for a transseries completion to the topological-string free energy of the form

$$(2.4) \quad F = \sum_{n=0}^{+\infty} \sigma^n e^{-nA(z)/g_s} F^{(n)}(g_s; z, \bar{z}),$$

where the (multi) instanton sectors $F^{(n)}(g_s)$ are also given by asymptotic series. In particular, it was found — both generically and in examples — that (2.4) has several nonperturbative sectors, with associated actions A_α , all of them holomorphic and determined by the CY geometry.

The transseries (2.4) was constructed by combining a nonperturbative interpretation of the holomorphic anomaly equations of [6] with the resurgence relations that transseries generically satisfy, such as, for example,

$$(2.5) \quad F_g^{(0)}(z, \bar{z}) \sim \frac{\Gamma(2g-1)}{A(z)^{2g-1}} F_0^{(1)}(z, \bar{z}), \quad \text{as } g \rightarrow +\infty.$$

Here $F_0^{(1)}$ is the first coefficient of the one-instanton series $F^{(1)}(g_s)$ and $A(z)$ is one of the instanton actions (the smallest one in absolute value, for the particular value of z). Subleading corrections to (2.5) lead to further multi-loop coefficients, $F_h^{(1)}$ with $h = 1, 2, \dots$. Generalizations of (2.5), now addressing the large-order behavior of the $F_g^{(n)}$ sequences, provide new constraints and relations between higher instanton coefficients.

This route towards the construction of (2.4), further developed in [35], draws a rather complete picture of what a transseries for $F(g_s)$ should look like. In principle, such a transseries should contain all nonperturbative information concerning the B-model, but also, via mirror symmetry [10], all A-model nonperturbative information. It is within this context that we shall set our attention upon structures of interest in algebraic and enumerative geometry, arising from the A-model set-up, in particular the case of enumerative GW invariants.

Let us spell out our strategy. The B-model construction (2.4) depends upon (z, \bar{z}) , the complex-structure moduli. From the standpoint of resurgence, these moduli may be regarded as external parameters, without any resurgent properties by themselves. But upon mirror symmetry, they relate the B-model CY threefold $\tilde{\mathcal{X}}$, with complex structure z , to the A-model mirror-CY threefold \mathcal{X} , with Kähler structure t . A functional relation $t = t(z)$ is then provided by the mirror map. This means that one may in fact compute the *mirror transseries* to (2.4), where its $F_g^{(0)}(t)$ components are nothing but the GW generating functions as in (1.2). Let us next focus on these enumerative invariants in greater detail, with the goal of uncovering which resurgent properties they carry, either intrinsic or merely inherited from the free energy.

2.1. Enumerative Gromov–Witten invariants

GW invariants count embeddings of Riemann surfaces of a given genus into a CY threefold \mathcal{X} , attending to the homology class of the image of this map. Thus, GW invariants are labelled by $g \in \mathbb{N}$, like the topological-string free energies, and $\beta \in H_2(\mathcal{X}, \mathbb{Z})$,

$$(2.6) \quad N_{g,\beta} \in \mathbb{Q}.$$

Akin to (1.2), they show up in the A-model perturbative free-energies through the expansion

$$(2.7) \quad F_g^{(0)} = \sum_{\beta \in H_2(\mathcal{X}, \mathbb{Z})} N_{g,\beta} Q^\beta.$$

Here we have used the mirror map to translate from complex structure moduli, z_i , to Kähler moduli, $t_i := -\log Q_i$ (roughly, the mirror map is $Q_i = \mathcal{O}(z_i)$). More precisely, if ω is the (complexified) Kähler form in \mathcal{X} and $[S_i]$, with $i = 1, 2, \dots, b_2(\mathcal{X})$, is a basis of $H_2(\mathcal{X}, \mathbb{Z})$, then one finds $\beta = \sum_i n_i [S_i]$ and $t_i := \int_{[S_i]} \omega$, in which case we may denote $Q^\beta = \prod_i Q_i^{n_i} = \exp(-\sum_i n_i t_i)$. In order to simplify things in the following, we shall restrict to examples where $b_2(\mathcal{X}) = 1$, in which case the sum over homology classes simplifies to

$$(2.8) \quad F_g^{(0)}(t) = \sum_{d=1}^{+\infty} N_{g,d} Q^d.$$

The index d is called the degree of the embedding. See, *e.g.*, [14] for more details on the relation between the enumerative GW invariants and their A-model generating functions.

Now (2.8) is a convergent series in Q , which, in particular, implies that it is *not* resurgent. Its non-vanishing radius of convergence is generically finite, due to a nearby singularity located at the so-called conifold locus [8]. This convergence may already suggest that the factorial growth of the free energies $F_g^{(0)}$ in genus must somehow arise from a combined contribution of several different degrees. We shall next try to understand how this might come about.

2.2. Growth of enumerative invariants in degree and in genus

As we introduce most of our main ideas, let us illustrate them with (partial) results from upcoming diverse examples. The simplest such example is naturally attached to the resolved conifold, for which the free energies can be computed exactly (see, *e.g.*, [48] for a review)

$$(2.9) \quad F_g^{(0),\text{coni}}(t) = (-1)^{g-1} \frac{B_{2g}}{2g(2g-2)!} \text{Li}_{3-2g}(e^{-t}), \quad g \geq 2,$$

where $\text{Li}_p(x)$ is the polylogarithm function. This immediately yields all GW invariants as

$$(2.10) \quad N_{g,d}^{\text{coni}} = f_g^{\text{coni}} d^{2g-3}, \quad f_g^{\text{coni}} := (-1)^{g-1} \frac{B_{2g}}{2g(2g-2)!}.$$

More interesting geometries we shall later address include the (non-compact) local \mathbb{P}^2 and the (compact) quintic CY threefolds, for which there are no such closed-form expressions. Enumerative invariants may, nonetheless, be generated on the computer to see in more detail how they grow in degree and genus. An example of the sort of numbers we have to work with is show in Figure 2, in the instance of local \mathbb{P}^2 (to be addressed in Section 4.1).

Growth in degree. Let us first consider the growth in degree at fixed genus. For the resolved conifold the answer is immediate from (2.10): it is given by the degree d , raised to a linear function of the genus g , namely $2g - 3$. For other, more intricate geometries the growth is similar but includes further parameters, such as a critical exponent γ which captures distinct topological-string universality classes, *i.e.*, distinct critical behaviors at the

$\log N_{g,d} $	20	21	22	23	24	25	26	27	28	29	30	31	32	33	34	35	36	37	38	39	40
20	111.4	117.1	122.6	128.0	133.2	138.3	143.4	148.3	153.2	157.9	162.6	167.3	171.8	176.3	180.8	185.2	189.5	193.9	198.1	202.3	206.5
21	113.7	119.6	125.3	130.8	136.2	141.4	146.6	151.6	156.6	161.5	166.3	171.0	175.7	180.3	184.8	189.3	193.7	198.1	202.5	206.8	211.1
22	116.0	122.0	127.9	133.5	139.1	144.5	149.7	154.9	160.0	165.0	169.9	174.7	179.5	184.2	188.8	193.4	197.9	202.4	206.8	211.2	215.5
23	118.2	124.4	130.4	136.2	141.9	147.4	152.8	158.1	163.3	168.4	173.4	178.4	183.2	188.0	192.8	197.4	202.0	206.6	211.1	215.6	220.0
24	120.4	126.7	132.9	138.9	144.7	150.3	155.9	161.3	166.6	171.8	177.0	182.0	187.0	191.8	196.7	201.4	206.1	210.7	215.3	219.9	224.4
25	122.5	129.0	135.3	141.5	147.4	153.2	158.9	164.4	169.9	175.2	180.4	185.6	190.6	195.6	200.5	205.4	210.1	214.9	219.5	224.2	228.7
26	124.5	131.2	137.7	144.0	150.1	156.0	161.8	167.5	173.1	178.5	183.9	189.1	194.3	199.3	204.3	209.3	214.1	219.0	223.7	228.4	233.0
27	126.5	133.4	140.0	146.5	152.7	158.8	164.8	170.6	176.2	181.8	187.2	192.6	197.8	203.0	208.1	213.1	218.1	223.0	227.8	232.6	237.3
28	128.5	135.5	142.3	148.9	155.3	161.5	167.6	173.5	179.3	185.0	190.6	196.0	201.4	206.7	211.9	217.0	222.0	227.0	231.9	236.8	241.6
29	130.4	137.6	144.6	151.3	157.9	164.2	170.4	176.5	182.4	188.2	193.9	199.4	204.9	210.3	215.6	220.8	225.9	231.0	236.0	240.9	245.8
30	132.2	139.6	146.7	153.7	160.4	166.9	173.2	179.4	185.4	191.3	197.1	202.8	208.4	213.8	219.2	224.5	229.7	234.9	240.0	245.0	249.9
31	134.0	141.6	148.9	155.9	162.8	169.5	175.9	182.2	188.4	194.4	200.3	206.1	211.8	217.4	222.9	228.2	233.6	238.8	244.0	249.1	254.1
32	135.7	143.5	151.0	158.2	165.2	172.0	178.6	185.1	191.4	197.5	203.5	209.4	215.2	220.9	226.4	231.9	237.3	242.7	247.9	253.1	258.2
33	137.4	145.4	153.0	160.4	167.6	174.5	181.3	187.8	194.3	200.5	206.6	212.7	218.5	224.3	230.0	235.6	241.1	246.5	251.8	257.1	262.3
34	139.0	147.2	155.0	162.6	169.9	177.0	183.9	190.6	197.1	203.5	209.7	215.9	221.9	227.7	233.5	239.2	244.8	250.3	255.7	261.0	266.3
35	140.6	149.0	157.0	164.7	172.2	179.4	186.4	193.3	199.9	206.4	212.8	219.0	225.1	231.1	237.0	242.8	248.4	254.0	259.5	265.0	270.3
36	142.2	150.7	158.9	166.8	174.4	181.8	188.9	195.9	202.7	209.3	215.8	222.2	228.4	234.5	240.4	246.3	252.1	257.7	263.3	268.8	274.3
37	143.7	152.4	160.7	168.8	176.6	184.1	191.4	198.5	205.5	212.2	218.8	225.3	231.6	237.8	243.8	249.8	255.7	261.4	267.1	272.7	278.2
38	145.1	154.0	162.6	170.8	178.7	186.4	193.9	201.1	208.2	215.0	221.8	228.3	234.7	241.0	247.2	253.3	259.2	265.1	270.9	276.5	282.1
39	146.6	155.6	164.3	172.7	180.8	188.7	196.3	203.7	210.8	217.8	224.7	231.4	237.9	244.3	250.6	256.7	262.8	268.7	274.6	280.3	286.0
40	147.9	157.2	166.1	174.6	182.9	190.9	198.6	206.2	213.5	220.6	227.6	234.3	241.0	247.5	253.9	260.1	266.3	272.3	278.3	284.1	289.9

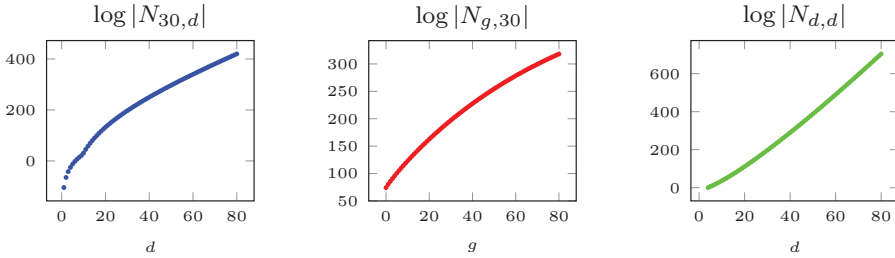


Figure 2. Sample of GW invariants for the local \mathbb{P}^2 CY threefold, alongside a visual representation of their growth with respect to degree d (in blue), genus g (in red), and a linear combination of the two (in green). Only in this latter case shall we find a factorial growth.

phase-transition point (see, *e.g.*, [43] for a discussion). In general one finds⁶ [4, 6, 41]

$$(2.11) \quad N_{g,d} \sim d^{(\gamma-2)(1-g)-1} e^{dt_c} (\log d)^{\alpha+\beta g}, \quad \text{as } d \rightarrow +\infty$$

(further including a possibly g -dependent pre-factor). In this expression, $e^{-t_c} = Q_c$ marks the radius of convergence of $F_g^{(0)}$ on the Q -plane. Expression (2.11) implies that the resolved conifold has $\gamma = 0$, being in the same universality class as, *e.g.*, the local \mathbb{P}^2 or the quintic CY threefolds. For example, for the quintic we have [4, 6]

$$(2.12) \quad N_{g,d}^{\text{quint}} \sim d^{2g-3} e^{dt_c} (\log d)^{2g-2},$$

where $t_c = 7.58995\dots$. For local \mathbb{P}^2 this growth is illustrated in the leftmost plot of Figure 2, at fixed genus $g = 30$. For very large degree d , the plotted

⁶Recall the notation where the boldface character specifies which index (if any) is the fixed one.

curve must tend to a straight line of slope $|t_c|$. On the other hand, for the family of local curves $X_p = \mathcal{O}(p-2) \oplus \mathcal{O}(-p) \rightarrow \mathbb{P}^1$ ($p \geq 3$) the critical exponent is instead $\gamma = -1/2$ [43], implying a distinct universality class and we shall discuss this example later in Section 4.3.

As mentioned earlier, the radius of convergence Q_c signals a singularity of the (free energy) generating function. Such critical points correspond to the points in moduli space where the A-model geometric interpretation breaks down, with a phase transition taking place from the large-radius (geometric) phase to a non-geometric phase. Near such a singularity,

$$(2.13) \quad F_g^{(0)} \sim c_g (Q_c - Q)^{(1-g)(2-\gamma)}, \quad g \geq 2.$$

Nearby Q_c all geometries within the same universality class will resemble each other, which implies that the coefficients c_g are universal. For example, for $\gamma = 0$ there is a double-scaling limit

$$(2.14) \quad g_s \rightarrow 0, \quad Q \rightarrow Q_c, \quad \text{with } \kappa := g_s (Q_c - Q)^{-1} \text{ fixed,}$$

such that

$$(2.15) \quad F^{(0)}(g_s; t) \rightarrow F_{\text{ds}}^{(0)}(\kappa) \simeq \sum_{g=2}^{+\infty} \frac{B_{2g}}{2g(2g-2)} \kappa^{2g-2},$$

which matches the $c = 1$ string at self-dual radius [8]. For other values of γ the coefficients c_g may be more complicated, being solutions to a nonlinear ODE such as Painlevé I, for example.

Growth in genus. As we turn towards understanding the dependence of GW invariants on genus, at fixed degree, $N_{g,d}$, it becomes useful to introduce the Gopakumar–Vafa (GV) invariants. These invariants are integer numbers, roughly counting the number of BPS states inside a CY threefold \mathcal{X} , and resulting from a reorganization of the A-model free energy as introduced in [49, 50]. The complete result involves a Schwinger-type computation which rewrites the free energy as an index that counts string-theoretic BPS states via an M-theory uplift, and which finally yields

$$(2.16) \quad \sum_{g=0}^{+\infty} g_s^{2g-2} F_g^{(0)}(Q) = g_s^2 c(t_i) + \ell(t_i) + \sum_{r=0}^{+\infty} \sum_{\beta} n_r^{(\beta)} \sum_{m=1}^{+\infty} \frac{1}{m} \left(2 \sin \frac{m g_s}{2} \right)^{2r-2} Q^{\beta m}.$$

Here, the $n_r^{(\beta)} \in \mathbb{Z}$ are the GV invariants, labeled by the Kähler class β and a spin index r . The polynomials $c(t_i)$ and $\ell(t_i)$ will play no role in the following.

It is straightforward to check that, generically, the GW invariants may be written explicitly in terms of the GV invariants as

$$(2.17) \quad N_{g,d} = \sum_{r=0}^g c_{r,g} \sum_{\beta|d} n_r^{(\beta)} \left(\frac{d}{\beta}\right)^{2g-3},$$

$$\text{using} \quad \left(2 \sin \frac{x}{2}\right)^{2r-2} =: \sum_{h=r}^{+\infty} c_{r,h} x^{2h-2}.$$

In here we already find the d^{2g-3} dependence which is characteristic of the resolved conifold. Now, an important property of the GV invariants, which will be useful in the following, is that for each degree d there is a specific genus, $G(d)$, after which all these invariants vanish, *i.e.*, $n_r^{(d)} = 0$ for $r > G(d)$ [50]. This function $G(d)$ is a polynomial in d , and this will simplify the dependence on g in (2.17) by replacing the upper limit in the r -sum; writing for all g

$$(2.18) \quad N_{g,d} = \sum_{r=0}^{G(d)} c_{r,g} \sum_{\beta|d} n_r^{(\beta)} \left(\frac{d}{\beta}\right)^{2g-3}.$$

In this expression the only remaining dependence upon the genus, g , lies in the coefficients $c_{r,g}$ and in the power of d/β . Since the coefficients $c_{r,g}$ are *independent* of the CY geometry, we should expect a generic formula to hold for the large growth of $N_{g,d}$ in genus. For example, as we shall discuss later on, for the case of local \mathbb{P}^2 and degree $d = 4$ we find

$$(2.19) \quad N_{g,d=4}^{\mathbb{P}^2} \sim (-1)^{g-1} \frac{B_{2g}}{2g(2g-2)!} 4^{2g-3} \left(3 - \frac{6}{2^{2g-3}} - \frac{192}{4^{2g-3}}\right) \\ + \frac{(-1)^{g-1}}{(2g-2)!} \frac{2^{2g-2}}{4} \left(120 + \frac{336}{2^{2g-2}}\right),$$

This formula, involving Bernoulli numbers and factorials, is actually *exact* for $g \geq 2$, not just a large- g approximation. The first numbers (3, -6, -192) can be recognized as the GV invariants $n_0^{(1)}$, $n_0^{(2)}$, and $n_0^{(4)}$ for local \mathbb{P}^2 , whereas the other (120, 336) are more complicated combinations involving higher-genera invariants. As such, in general, we can expect the following

formula to hold (see Appendix A for a proof)

$$(2.20) \quad N_{g,d} = f_g^{\text{coni}} \left\{ \sum_{n|d} a_n \left(\frac{d}{n}\right)^{2g-3} + \frac{2g}{B_{2g}} \frac{1}{d} \left(c_d \delta_{g,1} + \sum_{n=1}^{G(d)-1} b_{d,n} n^{2g-2} \right) \right\}.$$

where $a_d \equiv n_0^{(d)}$ and $b_{d,n}, c_d \in \mathbb{Z}$. In this expression the dependence on the genus g is explicit — one could even plug-in non-integer values of the genus after analytically continuing the Bernoulli numbers. If we fix the degree, as in $N_{g,d}$, it is then simple to see that the leading growth in genus is exponential, d^{2g-3} , with further subleading exponential and inverse-of-factorial corrections in g . The second plot in Figure 2 illustrates this genus dependence, at fixed degree $d = 30$, for local \mathbb{P}^2 . The plotted curve is asymptotic to a straight line of slope $2 \log d$.

Expression (2.20) shows how the contribution of GW invariants, $N_{g,d}$, to the free energies at a fixed single degree, d , again cannot be responsible for the factorial growth we need to find. In this way, the only option we have left to find the $\sim (2g)!$ factorial growth of the free energies, encoded in the GW invariants, is to address the *combined* growth in genus and degree.

Combined growth in genus and degree. Upon a second look at the (already familiar) characteristic behavior of GW invariants in d^{2g-3} , it should be straightforward to deduce that when d and g are linearly related, then the factorial growth is immediately realized. The link is the classical Stirling approximation,

$$(2.21) \quad n^n \sim \frac{n! e^n}{\sqrt{2\pi n}}.$$

Consider one more time the example of the resolved conifold in (2.10), and assume the dependence $d = a_0 + a_1 g$ for some values of a_0 and a_1 . Then, to leading order in g , one finds

$$(2.22) \quad N_{g,d=a_0+a_1g}^{\text{coni}} \sim \frac{\Gamma\left(2g - \frac{3}{2}\right)}{\left(\frac{4\pi}{e a_1}\right)^{2g - \frac{3}{2}}} \frac{\left(\frac{2e}{a_1}\right)^{\frac{3}{2}} e^{2\frac{a_0}{a_1}}}{2\pi^2}.$$

The factorial in g is now explicit and it comes from the term d^{2g-3} when $d = a_0 + a_1 g$. On the other hand, recall that the leading growth of the free

energy $F_g^{(0),\text{coni}}$ in this case is [24]

$$(2.23) \quad F_g^{(0),\text{coni}}(Q) \sim \frac{\Gamma(2g-1)}{(2\pi t)^{2g-1}} \frac{t}{\pi},$$

with instanton action $A = 2\pi t$. To connect this resurgence relation to the one in (2.22), one has to recall the definition of GW invariants (2.8)

$$(2.24) \quad F_g^{(0),\text{coni}} = \sum_{d=1}^{+\infty} N_{g,d}^{\text{coni}} Q^d,$$

and then notice that the largest contribution to this sum, for a fixed value of Q on the right-hand side, comes from

$$(2.25) \quad \frac{\partial}{\partial d} \left(N_{g,d}^{\text{coni}} Q^d \right) = 0 \quad \Rightarrow \quad d = \frac{2g-3}{t}.$$

So we should expect that taking $a_1 = 2/t$ and $a_0 = -3/t$ in (2.22) will reproduce something resembling (2.23). Indeed, one can easily check that we obtain the same instanton action as $\frac{4\pi}{a_1} = 2\pi t$ (where we ignore the exponential factor in (2.22) as such terms should be regrouped into the factor of Q^d in (2.24); *i.e.*, exponentials may be ignored when matching with (2.23)).

This strategy of selecting the leading contribution from the Q -expansion inside $F_g^{(0)}(Q)$ can be pushed further. One way to do so is to approximate the sum over the degree by an integration, and then perform a saddle-point approximation — and this will be a main theme throughout our analyses. Consider the following saddle-point approximation around $x = x_0$ (where $V'(x_0) = 0$),

$$(2.26) \quad \Phi(\lambda) = \int_0^{+\infty} dx e^{\lambda V(x)} \sim e^{\lambda V(x_0)} \sqrt{-\frac{2\pi}{\lambda V''(x_0)}} \left(1 + \mathcal{O}\left(\frac{1}{\lambda}\right) \right).$$

To apply this generic formula to our problem one just has to identify

$$(2.27) \quad \Phi(\lambda) \leftrightarrow F_g^{(0)}(Q), \quad e^{\lambda V(x)} \leftrightarrow N_{g,x} Q^x, \quad x \leftrightarrow d, \quad \lambda \propto g.$$

The only subtlety in this identification is that the saddle-point x_0 is also proportional to the coupling λ , as we saw for the resolved conifold (2.25). In any case, our goal is to solve for $e^{\lambda V(x_0)}$ in (2.26). Then, the only obstacle we have in order to do so is knowing the value of $V''(x_0)$. For the resolved conifold we had an explicit formula and, as such, we knew that

it was $-t/(a_0 + a_1g)^2$ where $x_0 = a_0 + a_1g$ and λ chosen the same; but in general there are no such explicit formulae. Nonetheless, let us postulate a completely similar dependence in g , namely

$$(2.28) \quad V''(x_0) \equiv -\frac{a_2(Q)}{\lambda^2} + \mathcal{O}\left(\frac{1}{\lambda^3}\right),$$

where we have chosen the explicit relation $\lambda = a_0 + a_1g$, and introduced the function $a_2(Q)$. If one makes further use of the leading large-order growth of the free energies [30],

$$(2.29) \quad \Phi(\lambda) = F_g^{(0)}(Q) \sim \frac{\Gamma(2g - \beta)}{A^{2g-\beta}} F_0^{(1)},$$

we finally obtain

$$(2.30) \quad N_{g,x_0} Q^{x_0}|_{x_0=a_0+a_1g} \sim \frac{\Gamma(2g - \beta - \frac{1}{2})}{A^{2g-\beta-\frac{1}{2}}} \left(\frac{a_2}{\pi a_1 A}\right)^{\frac{1}{2}} F_0^{(1)}.$$

Note that this large-order relation depends on a_1 and a_2 , functions of Q which define the position and shape of the saddle. For the resolved conifold, and even for other geometries with actions proportional to a Kähler parameter, we find that $a_1 = 2/t$ and $a_2 = t$. But for general geometries we do not know what these functions are or should be, and one has to run computational experiments in order to judiciously try to fix them. Note that once one approximates the sum over the degree by an integration, then different saddles will correspond to different leading actions, which may depend on the value of Q . For the resolved conifold there is only one leading action and one saddle. But for general geometries we can expect several of them — albeit one is always proportional to the Kähler parameter t . This is illustrated in Figure 3, where we have plotted saddles for the resolved conifold and local \mathbb{P}^2 (we shall discuss these plots in greater detail later on). The saddles are identified by numerically selecting, at fixed values of g and t but varying d , the GW invariants which contribute the most to the perturbative free energy. Both models clearly show a saddle associated to a Kähler action, with $A = 2\pi t$. For local \mathbb{P}^2 there is one further saddle, related to a conifold action, to be discussed in Section 4.1.

The main question. Let us finally address the main question motivating this paper. Are there nonperturbative extensions of the enumerative GW invariants — denote them by “ $N_{g,d}^{(n)}$ ”, with n an “instanton label” — just like there are nonperturbative extensions $F_g^{(n)}$ of the perturbative free energy?

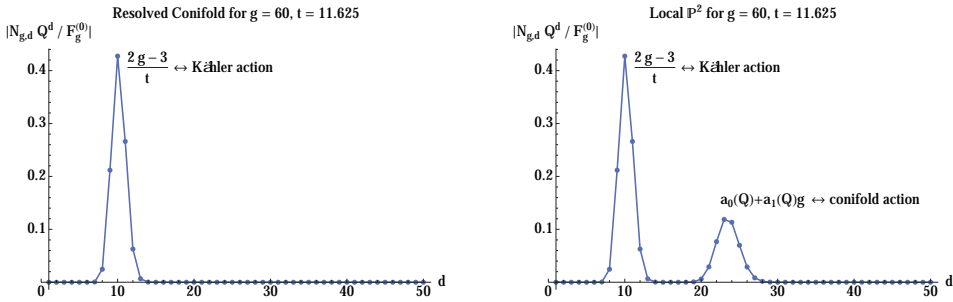


Figure 3. Graphical representation of which GW invariants contribute the most to a free energy $F_g^{(0)}(Q)$, for fixed values of g and $Q = e^{-t}$. This contribution is estimated by comparing the value of $N_{g,d} Q^d$, at different values of the degree d , against the total value of the genus- g perturbative free energy $F_g^{(0)}$. The resolved conifold, portrayed on the left, has a single saddle-point corresponding to the action $A = 2\pi t$; whereas for local \mathbb{P}^2 , portrayed on the right, an extra saddle-point attached to the conifold action is also present. These saddles may exchange dominance depending on the value of Q , but the set of leading degrees will always be in correspondence with the set of leading instanton actions.

And if so, what is their enumerative interpretation, *i.e.*, which counting problem is associated to these new numbers? An argument in favor of an affirmative answer arises from considering the A-model mirror to the B-model resurgent analysis of the free energy, and its associated transseries constructions [30, 32]. This procedure would certainly lead to an A-model transseries (and we shall illustrate this in the example of local \mathbb{P}^2), but the resulting transseries would not be an adequate generating function. In fact, while the perturbative $F_g(Q)$ is a natural generating function, collecting the GW invariants as a Q -expansion, the higher instanton sectors $F_g^{(n)}(t)$ will not be regular at $Q = 0$ and a naive Q -expansion is no longer an option. Then how do we extract the nonperturbative counterparts?

Schematically, we want to make sense of the following diagram

$$\begin{array}{ccc}
 F_g^{(0)} & \xrightarrow{\text{resurgence}} & F_g^{(n)} \\
 \downarrow \text{Q-expansion} & & \downarrow \text{expansion?} \\
 N_{g,d} & \xrightarrow{\text{resurgence + interpretation?}} & \text{“}N_{g,d}^{(n)}\text{”?}
 \end{array}
 \tag{2.31}$$

The left and upper arrows are well understood. The left arrow is just the A-model definition of GW invariants, while the upper arrow was made precise within the B-model set-up in [30, 32]. In this paper we try to take the first (exploratory) steps towards the definition of lower and right arrows, but a complete answer can only come with a geometric/enumerative interpretation of these conjectured quantities “ $N_{g,d}^{(n)}$ ”, which is beyond the scope of the present work.

What could these nonperturbative invariants “ $N_{g,d}^{(n)}$ ” be counting? With the nonperturbative sectors in the topological-string transseries naturally associated to D-brane sectors [22, 24], one possibility is that their counting is associated to embeddings of Riemann surfaces with boundaries, of certain genus and degree. These A-brane open-strings end in middle-dimensional lagrangian submanifolds (see, *e.g.*, [51]) and it is also possible that some counting associated to the corresponding target-space wrappings would play a part. But this type of counting is usually associated to the *open* GW invariants (see, *e.g.*, [52]), which means that — should this be the correct interpretation of the nonperturbative invariants — there may be an interesting link between closed and open GW invariants arising from relating perturbative and nonperturbative data in the topological-string transseries. Of course topological-string D-branes also relate to more intricate mathematical constructions, such as Fukaya and derived categories (see, *e.g.*, [53]), in which case the counting associated to the “ $N_{g,d}^{(n)}$ invariants” may be much more complicated.

Further note that, as GW invariants themselves have no transseries completions, we do not expect the lower arrow to be defined directly but rather as combination of left, upper, and right arrows (alongside the mirror map). In this way, one will have to extract the “ $N_{g,d}^{(n)}$ invariants” directly out of the nonperturbative sectors $F_g^{(n)}$. Now, the Q -expansion of the perturbative sector arises from a worldsheet-instanton expansion and thus naturally relates

to a counting problem. But the nonperturbative sectors lack such power-series expansions in Q (we shall soon illustrate in a couple of examples how they have singularities at $Q = 0$), implying that any nonperturbative GW invariants hidden inside the nonperturbative free-energies might be difficult to extract and their enumerative interpretation harder to decode (at the very least they will imply understanding how the aforementioned singularities come about, upon use of the mirror map). Furthermore, even after performing an asymptotic resurgent analysis of $N_{g,d}$, we have to disentangle the dependence in t , coming from the parameters a_0 and a_1 , in the linear dependence between degree and genus. At the end of the day, this leaves the right arrow to be defined. What one has to do is to understand, via mirror symmetry, how to relate nonperturbative multi-loop multi-instanton coefficients in the B-model transseries, to the nonperturbative sectors appearing in the asymptotic resurgence relations for the combined genus/degree growth of GW invariants.

Our goal in this paper is to initiate this line of research, computationally exploring diverse CY examples. We try to identify the structure of these new invariants, as they are encoded in the nonperturbative content of the A-model free energy, but shall leave open their subsequent enumerative interpretation for future research.

3. An exactly-solvable model: the resolved conifold

This section addresses our first example, concerning an exactly solvable model: the resolved conifold. This toric variety is a non-compact CY threefold which is the total space of the bundle $\mathcal{O}(-1) \oplus \mathcal{O}(-1) \rightarrow \mathbb{P}^1$. The perturbative free-energy for the resolved conifold can be computed exactly to all orders in the genus expansion (see, *e.g.*, [48] and references therein). This of course translates to the fact that one may obtain analytical expressions for all its (infinite) GW invariants [54]. For any genus g , the results are

$$(3.32) \quad F_0^{(0)} = \frac{t^3}{12} - \frac{\pi^2 t}{6} + \zeta(3) - \text{Li}_3(e^{-t}),$$

$$(3.33) \quad F_1^{(0)} = -\frac{t}{24} + \zeta'(-1) + \frac{1}{12} \text{Li}_1(e^{-t}),$$

$$(3.34) \quad F_g^{(0)} = \frac{B_{2g} B_{2g-2}}{2g(2g-2)(2g-2)!} + (-1)^{g-1} \frac{B_{2g}}{2g(2g-2)!} \text{Li}_{3-2g}(e^{-t}), \quad g \geq 2,$$

where $\text{Li}_p(z)$ is the polylogarithm of index p . In the following we will drop the contribution from the constant map [54, 55] and mostly focus on the large-order contributions $g \geq 2$.

Due to the polylogarithm these free energies grow factorially in the genus and lead to an asymptotic, Gevrey-1 perturbative free-energy [47]. The resurgent properties of this series have been studied in detail in [24, 33], with the result

$$(3.35) \quad F_g^{(0)} \sim \sum_{n=1}^{+\infty} \sum_{m \in \mathbb{Z}} \left\{ \frac{\Gamma(2g-1)}{(nA_m)^{2g-1}} \frac{A_m}{2\pi^2 n} + \frac{\Gamma(2g-2)}{(nA_m)^{2g-2}} \frac{1}{2\pi^2 n^2} \right\},$$

where $A_m(t) = 2\pi(t + 2\pi im)$ are the instanton actions. For our purposes, we shall focus on the *leading* contribution, whose action is $A = 2\pi t$, in which case

$$(3.36) \quad F_g^{(0)} \sim \frac{\Gamma(2g-1)}{A^{2g-1}} \frac{A}{2\pi^2}.$$

Let us next translate these resurgent properties to the level of GW invariants.

The GW invariants for the resolved conifold can be immediately read from the free energies, by simply expanding the polylogarithm in power series. One finds

$$(3.37) \quad N_{g,d}^{\text{coni}} = f_g^{\text{coni}} d^{2g-3},$$

where f_g^{coni} includes the Bernoulli dependence and is defined in (2.10). These invariants have such a simple form, given that they are actually generated by a single non-vanishing GV invariant

$$(3.38) \quad n_0^{(1)} = 1.$$

Likewise, the *abc*-coefficients we introduced in (2.20) vanish except for the one which equals the GV invariant, $a_1 = n_0^{(1)} = 1$. This makes this geometry considerably simpler than the ones we shall explore later, allowing for an analytic treatment whose features will also show up later.

As we anticipated in some detail in the previous section, the factorial growth of the free energy arises from the term d^{2g-3} when d grows linearly with g . This is completely precise when the degree is a saddle point, in the sense explained earlier. This point, $d = (2g - 3)/t$, was computed in equation (2.25) and graphically represented in Figure 3 (left plot). One caveat about the saddle-point approximation is that generically the saddle-point lands

on non-integer values of the degree. In order to be able to do numerical analyses with actual GW invariants, we look at nearby (integer) values of the degree. A practical computational choice, one that we will also use for other geometries, is to set

$$(3.39) \quad g = \frac{t}{2}d + q, \quad \text{with} \quad - \left\lfloor \frac{t}{4} - \frac{3}{2} \right\rfloor \leq q \leq \left\lfloor \frac{t}{4} + \frac{3}{2} \right\rfloor,$$

and set t to an even integer (and q must consequentially be an integer).

Since in this example there is an analytic expression for all GW invariants, we can use it to obtain the resurgence relation

$$(3.40) \quad f_g^{\text{coni}} d^{2g-3} Q^d \Big|_{g=\frac{t}{2}d+q} \sim \sum_{h=0}^{+\infty} \frac{\Gamma(2g - \frac{3}{2} - h)}{(2\pi t)^{2g - \frac{3}{2} - h}} \frac{t^{\frac{3}{2} - h}}{2^{2h+1} \pi^{h+2}} \mathcal{P}_h(q).$$

This expression is obtained by making use of the following asymptotic formulae (for large degree d and genus g):

$$(3.41) \quad f_g^{\text{coni}} \Big|_{g=\frac{t}{2}d+q} \sim 2 \frac{2g - 1}{(2\pi)^{2g}} \zeta(2g),$$

$$(3.42) \quad d^{2g-3} \Big|_{g=\frac{t}{2}d+q} \sim \frac{e^{td}}{\sqrt{2\pi}} \frac{\Gamma(2g - \frac{5}{2})}{t^{2g-3}} \sum_{n=0}^{+\infty} \frac{\varrho_n(q)}{(td)^n},$$

where $\varrho_n(p)$ is a polynomial of degree $2n$ in q . As to the polynomials $\mathcal{P}_h(q)$ in (3.40) above, these are polynomials in q of degree $2h$ with rational⁷ coefficients. The first of which are

$$(3.43) \quad \mathcal{P}_0(q) = 1,$$

$$(3.44) \quad \mathcal{P}_1(q) = -\frac{71}{12} + 12q - 4q^2,$$

$$(3.45) \quad \mathcal{P}_2(q) = \frac{11545}{288} - 131q + \frac{419q^2}{3} - \frac{176q^3}{3} + 8q^4,$$

$$(3.46) \quad \mathcal{P}_3(q) = -\frac{17534803}{51840} + \frac{33553q}{24} - \frac{157393q^2}{72} + \frac{15220q^3}{9} - \frac{2062q^4}{3} + \frac{416q^5}{3} - \frac{32q^6}{3},$$

⁷This depends on the way they are presently written. It is simple to note that the denominators in the first terms of the polynomials, the numbers (1, 12, 288, 51840), correspond to the denominators that appear in the asymptotic expansion of the Gamma-function. In particular, we could rewrite (3.43) through (3.46) by pulling out these overall factors, in which case we would then find a set of polynomials with integer coefficients.

and in general they are such that they make the following asymptotic expansion hold for any q as $x \rightarrow +\infty$,

$$(3.47) \quad \sqrt{2\pi} e^{2q-x} (x-1)(x-2q)^{x-3} \sim \sum_{h=0}^{+\infty} \Gamma\left(x - \frac{3}{2} - h\right) 2^{-h} \mathcal{P}_h(q).$$

Note that expression (3.40) conforms to the usual resurgence relations, which, for some generic free-energy perturbative expansion, look like (see, *e.g.*, [20] for an introduction)

$$(3.48) \quad \begin{aligned} F_g^{(0)} &\sim \sum_{n=1}^{+\infty} \frac{\Gamma(2g-n\beta)}{(nA)^{2g-n\beta}} \frac{S_1^n}{2\pi i} \sum_{h=0}^{+\infty} \frac{\Gamma(2g-n\beta-h)}{\Gamma(2g-n\beta)} F_h^{(n)} (nA)^h \\ &= \frac{\Gamma(2g-\beta)}{A^{2g-\beta}} \frac{S_1}{2\pi i} \left(F_0^{(1)} + \frac{A}{2g-\beta-1} F_1^{(1)} \right. \\ &\quad \left. + \frac{A^2}{(2g-\beta-1)(2g-\beta-2)} F_2^{(1)} + \dots \right) \\ &\quad + \frac{\Gamma(2g-2\beta)}{(2A)^{2g-2\beta}} \frac{S_1^2}{2\pi i} \left(F_0^{(2)} + \frac{2A}{2g-2\beta-1} F_1^{(2)} + \dots \right) \\ &\quad + \mathcal{O}(3^{-2g}). \end{aligned}$$

Indeed, in (3.40) one immediately identifies the $\sim (2g)!$ growth, alongside the instanton action $A = 2\pi t$ which is the *same* action that appears in the free energies. Of course (3.40) also has higher instanton corrections which improve the asymptotics further as in the above expression. These arise from including the (exponentially) subleading terms in $\zeta(2g) = \sum_{n=1}^{+\infty} n^{-2g}$ in the large- g expansion of the Bernoulli numbers, B_{2g} , in (2.10); and from computing the complete large- d transseries expansion of $d^{td+2q-3}$. The result is

$$(3.49) \quad f_g^{\text{coni}} d^{2g-3} Q^d \Big|_{g=\frac{t}{2}d+q} \sim \sum_{n=1}^{+\infty} \sum_{h=0}^{+\infty} \frac{\Gamma(2g - \frac{3}{2} - h)}{(nA)^{2g - \frac{3}{2} - h}} \frac{t^{\frac{3}{2}-h}}{2^{2h+1} \pi^{h+2} n^{\frac{3}{2}+h}} \mathcal{P}_h(q).$$

Some computational tests on the validity of (3.40) are shown in Figures 4 and 5. Figure 4 presents a test of the instanton action. We plot the analytical $A_K = 2\pi t$ against numerical tests of this action. We use the standard

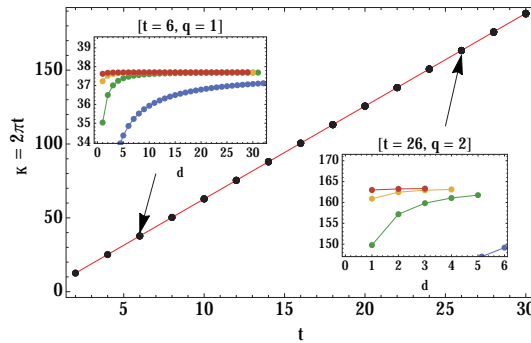


Figure 4. Test of the instanton action $A_K = 2\pi t$, from the Kähler saddle-point, for the resolved conifold. The inclosed plots show the convergence for a couple of values of t and q .

techniques of Richardson extrapolation/Richardson transforms⁸ to accelerate convergence (similar to tests done in, *e.g.*, [22]). An illustration of these transforms for different values of t and q is shown in the inclosed figures, where the original sequence is shown in blue together with its first (green), second (yellow) and third (red) Richardson transforms. We do this for varying t (the horizontal axis) but also varying q , *i.e.*, each black dot is actually several overlapping black dots, each one the third Richardson transform of the numerical sequence for the instanton action, for that particular value of t and for a range of different values of q . Then Figure 5 tests the validity of (3.43) through (3.46) (in fact up to $h = 5$), this time around for fixed q . Each inverted triangle in the plot is again the third Richardson transform of the tested sequence. All these plots very cleanly illustrate the validity of (3.40).

In Section 2 we showed how to relate GW asymptotics to free-energy instanton sectors, in particular relating the first term in the right-hand side of (3.40) with the one-loop one-instanton free energy $F_0^{(1)}$; see (2.30) and the discussion which follows. Ideally, one would now like to do the same

⁸Given a k -sequence $\mathbb{S}(k) \simeq s_0 + \frac{s_1}{k} + \frac{s_2}{k^2} + \dots$, its n -th Richardson transform is defined as

$$(3.50) \quad \text{RT}_{\mathbb{S}}(k, n) = \sum_{m=0}^n (-1)^{m+n} \frac{(k+m)^n}{m!(n-m)!} \mathbb{S}(k+m).$$

Convergence is accelerated by cancellation of subleading terms in the original sequence up to k^{-n} order.

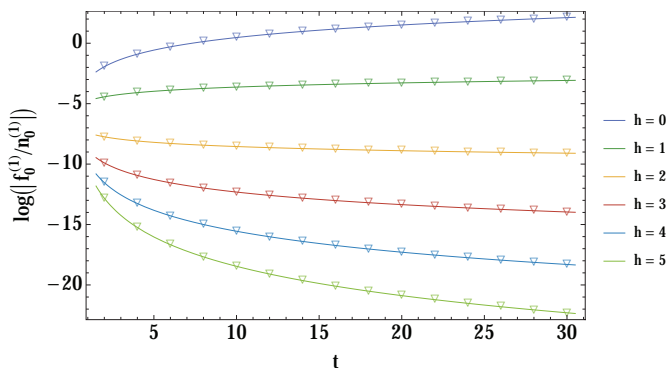


Figure 5. Numerical check of the loop-corrections $f_h^{(1)} := \frac{n_0^{(1)} t^{\frac{3}{2}-h}}{2^{2h+1} \pi^{h+2}} \mathcal{P}_h(q)$, for $h = 0, \dots, 5$ and $q = 1$, for the resolved conifold. We plot the logarithm of the ratio $f_0^{(1)}/n_0^{(1)}$ so that all curves fit within the same graph (and where the GV invariant is $n_0^{(1)} = 1$).

for the multi-loop (eventually multi-instanton) one-instanton free energies and their relation to higher terms in (3.40). Unfortunately, already finding a direct relation at two-loops, between $F_1^{(1)}$ and any higher term in (3.40), turns out not to be possible using the saddle-point approximation from Section 2. In fact, our saddle-point approach is non-standard, in the sense that the saddle-point itself grows with d (or g), which essentially obscures a clear-cut relation between free-energy asymptotics and GW asymptotics beyond the first term. For the present example of the resolved conifold we can bypass this problem, working directly with the explicit form of the GW invariants, but this will not be possible for more complicated examples.

Let us end our discussion of the resolved conifold by going back to our diagram (2.31). As we mentioned earlier, one cannot find nonperturbative GW invariants via a Q -expansion of the resurgent asymptotic expansion for the perturbative free energy $F_g^{(0)}$. This is already clear in equation (3.36), where, although the left-hand side does have a regular expansion around $Q = 0$ from which one reads the GW invariants (this is just the statement that the left-hand side is a regular generating function), the same does not hold true for the right-hand side, where one finds a logarithmic singularity at that same point (recall that the instanton action is proportional to t). In other words, the “resurgence rewriting” of the perturbative free energies, $F_g^{(0)}(Q)$, as an asymptotic series in $1/g$ does not respect, term by term, a regular Q -expansion. Only when we consider all corrections in $1/g$ and

perform their resummation (yielding the polylogarithm, in this case of the resolved conifold) can we recover regularity at $Q = 0$. Looking directly at the resurgent GW expansion (3.40), one also sees how the right-hand side has a non-regular Q -dependence through $t = -\log Q$. Although the possibility remains that there might be a better variable than Q or t to establish the match against nonperturbative GW invariants, it may also be the case that there is no such variable and reading nonperturbative GW invariants (naturally formulated using a Q -expansion) from resurgence expressions (naturally written using the t variable) is in fact a nontrivial problem which might require some *a priori* enumerative interpretation to know what to look for. Perhaps the fact that the polynomials (3.43) through (3.46), appearing in the resurgence relation (3.40), have rational coefficients much like the GW invariants themselves, is a clue in that direction.

4. Computational explorations in Calabi–Yau threefolds

We shall now move on towards non-trivial geometries, for which there are no closed-form expressions for enumerative GW invariants. We shall instead resort to computational methods in order to explore their asymptotics and resurgent structures.

4.1. The example of local \mathbb{P}^2

Our first non-trivial example will be a local-surface toric-variety. We start with the non-compact CY threefold known as local \mathbb{P}^2 , which is the total space of the line bundle $\mathcal{O}(-3) \rightarrow \mathbb{P}^2$. This example of local \mathbb{P}^2 has a single complex modulus z , and a mirror map of the schematic form $Q = e^{-t} = \mathcal{O}(z)$, which eventually allows for a calculation of GW invariants [41, 56] (the resulting Kähler modulus being the size of the \mathbb{P}^2). In fact, the large-order data for the resurgence analysis first arises in the B-model and will thus require translation into A-model expressions. Specifically, the high genus GW invariants for local \mathbb{P}^2 will come out of B-model calculations, both perturbative [57] and nonperturbative [30, 32], followed by mirror symmetry [10].

Free energies and Gromov–Witten invariants. The perturbative free energies are best computed within the B-model using the holomorphic anomaly equations, which are recurrence relations in the genus [6, 58]. The GW invariants are then extracted using the mirror map back to the A-model, and removing the anti-holomorphic dependence (in \bar{z}) which is introduced

by this computation. We shall not get into any details, which may be found in [57], but it is perhaps worth mentioning the Picard–Fuchs equation. Its solutions, the periods, are the source to the genus-zero free energy, the mirror map, and also the instanton actions [27]. For local \mathbb{P}^2 , the Picard–Fuchs equation is

$$(4.51) \quad \left\{ (z\partial_z)^3 + 3z^2 \partial_z (3z\partial_z + 1) (3z\partial_z + 2) \right\} f(z) = 0.$$

One of its three independent solutions is a constant. Another one, having a $\log z$ singularity, can be identified as the mirror map,

$$(4.52) \quad \log Q = -t = \log z - 6z + 45z^2 - 560z^3 + \dots.$$

The last solution, having a $\log^2 z$ singularity, can be associated to $\partial_t F_0^{(0)}$. Upon integration of this last solution, and use of the mirror map, one finds the genus-zero free energy as

$$(4.53) \quad F_0^{(0)} = c_3 t^3 + c_2 t^2 + c_1 t + 3Q - \frac{45}{8} Q^2 + \frac{244}{9} Q^3 + \dots.$$

One can ignore the coefficients c_i and then read the GW invariants, $N_{0,d}$, from this Q -series.

Within the B-model, the higher-genus free energies⁹, $F_g^{(0)}$, may be compactly written as polynomials in z and $S^{zz}(z, \bar{z})$, an auxiliary variable called the propagator [59]. To extract higher-genus GW invariants one has to use the holomorphic limit of the propagator S^{zz} (in the large-radius frame),

$$(4.54) \quad S_{\text{hol, [LR]}}^{zz} = \frac{1}{2} Q^2 + 15Q^3 + 135Q^4 + \dots.$$

Consider for example $F_2^{(0)}(z, S^{zz})$, which follows from the holomorphic anomaly equations as

$$(4.55) \quad F_2^{(0)} = \left(-\frac{1}{3z^3(1+27z)} \right)^2 \left(\frac{5}{24} (S^{zz})^3 - \frac{3z^2}{16} (S^{zz})^2 + \frac{z^4}{16} S^{zz} - \frac{(11 - 162z - 729z^2) z^6}{1920} \right) - \frac{1}{1920}.$$

⁹Note that the genus-one free energy is calculated separately (see [58] for details), and further has a direct relation to the propagator; namely $\partial_z F_0^{(1)} = \frac{1}{2} C_{zzz} S^{zz}$, where $C_{zzz} = (-3z^3(1+27z))^{-1}$ is the Yukawa coupling computed out of the Picard–Fuchs equation.

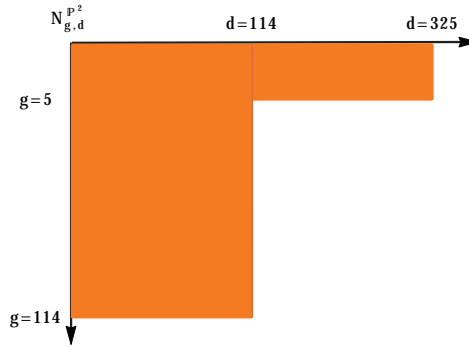


Figure 6. Maximum degree and genus of the GW invariants we computed for local \mathbb{P}^2 .

Taking the holomorphic limit and using the mirror map, $z = z(Q)$, one then obtains the A-model result

$$(4.56) \quad F_2^{(0)} = \frac{1}{80}Q + \frac{3}{20}Q^3 - \frac{514}{5}Q^4 + \dots .$$

Here, the coefficients of the Q -expansion are the $N_{2,d}$ GW invariants. In this way, the holomorphic anomaly equations systematically compute $F_g^{(0)}$, out of $F_h^{(0)}$ with $h = 1, \dots, g - 1$, and from them one extracts the $N_{g,d}$ GW invariants as described above. An illustrative (*i.e.*, partial) table of GW invariants for local \mathbb{P}^2 may be found in Appendix B.1. In Figure 6 we schematically represent all the GW invariants we have computed and work with in the present paper.

As studied in great detail in [30, 32] the free energies for local \mathbb{P}^2 , $F_g^{(0)}$, grow factorially fast and render the free-energy expansion asymptotic. The resurgent structure which was uncovered in those references may be summarized as follows. There are several instanton actions, labelled by A_1 , A_2 , A_3 and A_K , which give rise to corresponding nonperturbative sectors within the total free-energy transseries. Out of these, two actions are leading at large-order, these are A_1 and A_K , meaning that for some values of the complex-structure modulus z they are the actions controlling the leading growth of the $F_g^{(0)}$. Around the large-radius point in moduli space, $z = 0$, it is $A_K = 2\pi t(z)$ which is leading, and elsewhere it is $A_1 = \frac{2\pi i}{\sqrt{3}} T_c(z)$, where

$T_c(z) = 12\sqrt{3}\pi^2 i \partial_t F_0^{(0)}$ is the flat coordinate¹⁰ around the conifold point $z = -1/27$. For obvious reasons, we name A_K as the Kähler action and A_1 as the conifold action (in fact also A_2 and A_3 are related to the conifold point, but they will not play any role in the present paper).

In this case, the large-order growth of the free energies may be either

$$(4.57) \quad F_g^{(0)} \sim \frac{\Gamma(2g-1)}{A_1^{2g-1}} F_0^{(1)[c]} \quad \text{or} \quad F_g^{(0)} \sim \frac{\Gamma(2g-1)}{A_K^{2g-1}} F_0^{(1)[K]},$$

depending on the value of Q . The one-loop one-instanton coefficients are computed from an extension of the holomorphic anomaly equations, alongside the above resurgent relations (which were needed in order to fix the holomorphic anomaly). They are part of the B-model transseries, and one finds [32]

$$(4.58) \quad F_0^{(1)[c]} = \frac{A_1}{2\pi} e^{\frac{1}{2}(\partial_z A_1)^2 (S_{\text{hol},[LR]}^{zz} - S_{\text{hol},[c]}^{zz})} \quad \text{and} \quad F_0^{(1)[K]} = \frac{3A_K}{2\pi^2}.$$

The left expression involves $S_{\text{hol},[LR]}^{zz}$, whose Q -expansion was written in (4.54), but it also involves the holomorphic limit of the propagator in the conifold frame, $S_{\text{hol},[c]}^{zz}$ (see [32]). It is interesting to note how the expression on the right of (4.58) is actually equivalent, up to a factor of $3 = n_0^{(1)}$, to the one we computed earlier for the resolved conifold.

Being part of the B-model transseries, one may feel tempted to use the mirror map and write these nonperturbative expressions in the A-model, hoping for regular generating functions of our would-be nonperturbative invariants. Unfortunately, as already explained earlier, their Q -expansions are explicitly non-regular

$$(4.59) \quad F_0^{(1)[c]} = \frac{i(-Q)^{\frac{3}{2}}}{4\pi} \left((\log(Q) - i\pi)^2 - \pi^2 - 18Q + \frac{135}{2}Q^2 + \dots \right) \\ \times \left(1 - \frac{27}{2}Q + \frac{1539}{8}Q^2 + \dots \right), \\ F_0^{(1)[K]} = -\frac{3}{\pi} \log Q.$$

This implies that the A-model transseries, obtained via mirror map from the B-model transseries, is not a regular generating function and one has to

¹⁰References [30, 32] used the notation t_c for this flat coordinate. Herein we use T_c instead so as not to clash with our conifold critical point.

dig deeper in order to try to understand the counting problem associated to the conjectured quantities “ $N_{g,d}^{(n)}$ ”.

Analysis of large-degree growth. At fixed genus, the GW invariants grow exponentially in the degree as

$$(4.60) \quad N_{g,d} \sim c_g d^{2g-3} e^{dt_c} (\log d)^\delta,$$

where $t_c := t(z = -1/27) = 2.90759\dots - i\pi$ [41, 60]. Figure 7 shows a numerical verification of this value for t_c . The exponent $2g - 3$ of the degree d may be verified numerically from the following large- d sequence

$$(4.61) \quad f_d - 2fd^2 \sim 2g - 3, \quad \text{where} \quad f_d := d \left(e^{t_c} \frac{N_{g,d+1}}{N_{g,d}} - 1 \right).$$

Due to the presence of the d^2 factor, and the limit upon available data, the results are not as good as those for t_c . Nonetheless, this exponent may also be cleanly verified numerically, as it is shown in Figure 8. Finally, in similar fashion, we can determine the power of the logarithm $\log d$ from the sequence

$$(4.62) \quad 2^\delta \sim \frac{e^{d(d-1)t_c} N_{g,d^2}}{d^{2g-3} N_{g,d}}.$$

This is done in Figure 9, where it is shown that this exponent may be well fitted to the expected $\delta = 2g - 2$. Unfortunately, our available data does not allow us to numerically compute the genus-dependent pre-factor c_g with enough accuracy as to present it here.

Analysis of large-genus growth. As explained in Section 2, the large-genus expansion is best expressed in terms of the coefficients a_d , $b_{d,n}$, and c_d , as in (2.20), which we reproduce in here

$$(4.63) \quad N_{g,d}^{\mathbb{P}^2} = f_g^{\text{coni}} \left\{ \sum_{n|d} a_n^{\mathbb{P}^2} \left(\frac{d}{n} \right)^{2g-3} + \frac{2g}{B_{2g}} \frac{1}{d} \left(c_d^{\mathbb{P}^2} \delta_{g,1} + \sum_{n=1}^{G_{\mathbb{P}^2}(d)-1} b_{d,n}^{\mathbb{P}^2} n^{2g-2} \right) \right\},$$

and where, for this example, one explicitly has $G_{\mathbb{P}^2}(d) = (d - 1)(d - 2)/2$. A table with these first few coefficients is shown in Appendix B.1. Recall that these are just convenient integer numbers which essentially capture the very same information as either GW or GV invariants.

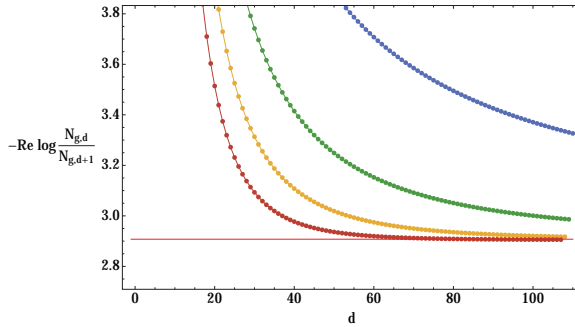


Figure 7. Local \mathbb{P}^2 : The exponent t_c in the growth of $N_{g,d}$ is captured from the ratio of two consecutive GW invariants, when the degree is large. We plot that ratio alongside three Richardson extrapolations, which are clearly converging faster towards the expected result (up to a numerical relative error of about 0.06%).

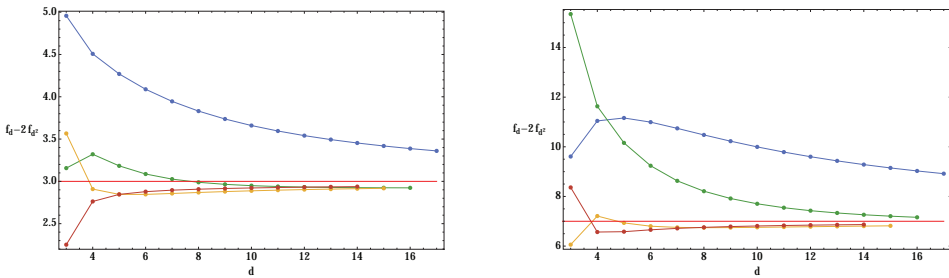


Figure 8. Local \mathbb{P}^2 : The exponent $2g - 3$ is the leading large-order term in $f_d - 2f_{d^2}$. We have data up to $d = 325$ so that the horizontal axis can only reach $d = 17$. The plots illustrate the first few Richardson transforms for $g = 3$ (left) and $g = 5$ (right), converging faster towards the expected result (up to numerical relative errors of about 2% in both cases). Notice how the presence of logarithms in (4.60) makes the convergence of Richardson transforms much slower.

Some of these coefficients, $b_{d,n}$ with n close to $G_{\mathbb{P}^2}(d) - 1$, can be identified in closed form as

$$(4.64) \quad b_{d,G_{\mathbb{P}^2}(d)-1-k}^{\mathbb{P}^2} = p_{-3}(k) (-1)^d d ((d+1)(d+2) - 2k), \\ 0 \leq k \leq d - 2,$$

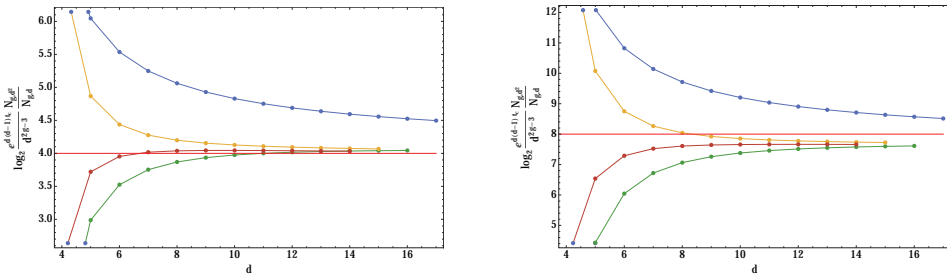


Figure 9. Local \mathbb{P}^2 : The exponent δ of the logarithm $\log d$ is the leading term in the sequence (4.62). Having data up to $d = 325$ implies the horizontal axis only reaches $d = 17$. We plot the first few Richardson transforms for $g = 3$ (left) and $g = 5$ (right), converging faster towards the expected result (up to small numerical relative errors of about 3% and 4%, respectively).

where the $p_{-3}(k)$ are given by the generating function

$$(4.65) \quad \sum_{k=0}^{+\infty} p_{-3}(k) q^k = \prod_{m=1}^{+\infty} \frac{1}{(1 - q^m)^3}.$$

For larger values of k one can try to extend the above formula, at the cost of identifying similar coefficients to $p_{-3}(k)$. A conjectural partial formula for $b_{d,n}^{\mathbb{P}^2}$ is

$$(4.66) \quad b_{d,G_{\mathbb{P}^2}(d)-1-k}^{\mathbb{P}^2} \stackrel{?}{=} (-1)^d d \sum_{s=0}^{+\infty} (\alpha_{s,k-m_s d+n_s} (d+1-s)(d+2-s) - \beta_{s,k-m_s d+n_s}),$$

where

$$(4.67) \quad \begin{aligned} m_0 = 0, \quad n_0 = 0, \quad \alpha_{0,n} = p_{-3}(n), \quad \beta_{0,n} = 2np_{-3}(n), \\ m_1 = 1, \quad n_1 = 1, \quad \sum_{n=0}^{+\infty} \alpha_{1,n} q^n = -3 \frac{1+q+q^2}{1-q} \prod_{m=1}^{+\infty} \frac{1}{(1-q^m)^3}, \end{aligned}$$

$$(4.68) \quad -\beta_{1,n} = 0, 18, 144, 684, 2484, 7578, 20628, 51390, 119736, 263970, 556308, 1127880, 2212704, ?,$$

$$(4.69) \quad \begin{aligned} m_2 = 2, \quad n_2 = 4, \quad -\alpha_{2,n} = 6, 24, 72, 162, 315, ?, \\ -\beta_{2,n} = 0, 36, 252, 1008, 3042, ?. \end{aligned}$$

This is as far as we were able to reach with the data we have available for local \mathbb{P}^2 .

Combined/diagonal large-growth in genus and degree. As discussed earlier in Section 2, and illustrated in Figure 3, local \mathbb{P}^2 has two (different) growths of combined genus and degree. They are associated to the Kähler ($A_K = 2\pi t$) and conifold (A_c) instanton actions, and they are, respectively,

$$(4.70) \quad d = \frac{2g - 3}{t} \quad \text{and} \quad d = a_0(Q) + a_1(Q)g.$$

Note that, as one varies t , the large-order growth of the free energies will be dominated by either A_K or A_c , or a competition between both (see the analysis in [32]). The situation is slightly different with the GW large-order. Here, along *any* diagonal one will find a factorial growth. However, from a resurgence standpoint, perhaps the most interesting diagonals are the ones which connect back to the resurgent structure of the free energies [30, 32]. For any chosen diagonal, this connection will exist every time there is a value of t which realizes that chosen diagonal as one of the above (specific) slices. If such a value of t exists, then the large-order growth of the enumerative invariants will be dominated by either A_K or A_c and the connection to the free energies is rather clean. If not, one will instead be upon a “mixed” diagonal with both A_K and A_c vying for dominance. Below we shall focus only upon the leading diagonals.

The first leading degree above was explored and justified analytically for the resolved conifold, and the main features which were found in that example remain in the present one. The second leading degree above depends on t (or Q) through two *unknown* functions, $a_0(Q)$ and $a_1(Q)$. At this stage, these functions may only be accessed via *numerical* computations; and given limited data, with some significant limitations. In the following we shall summarize the resulting factorial growth of the GW invariants, along the leading diagonals of their (g, d) -table, and the relation of this growth with the resurgent structure of the topological-string free energy.

Kähler leading degree. In this case, the only difference with respect to the resolved conifold turns out to be a simple multiplying factor, the GV invariant $n_0^{(1)} = 3$ of local \mathbb{P}^2 , in which case the analog of (3.40) is now

$$(4.71) \quad N_{g,d}^{\mathbb{P}^2} Q^d \Big|_{g=\frac{t}{2}d+q} \sim \sum_{h=0}^{+\infty} \frac{\Gamma(2g - \frac{3}{2} - h)}{A_K^{2g - \frac{3}{2} - h}} \frac{n_0^{(1)} t^{\frac{3}{2} - h}}{2^{2h+1} \pi^{h+2}} \mathcal{P}_h(q).$$

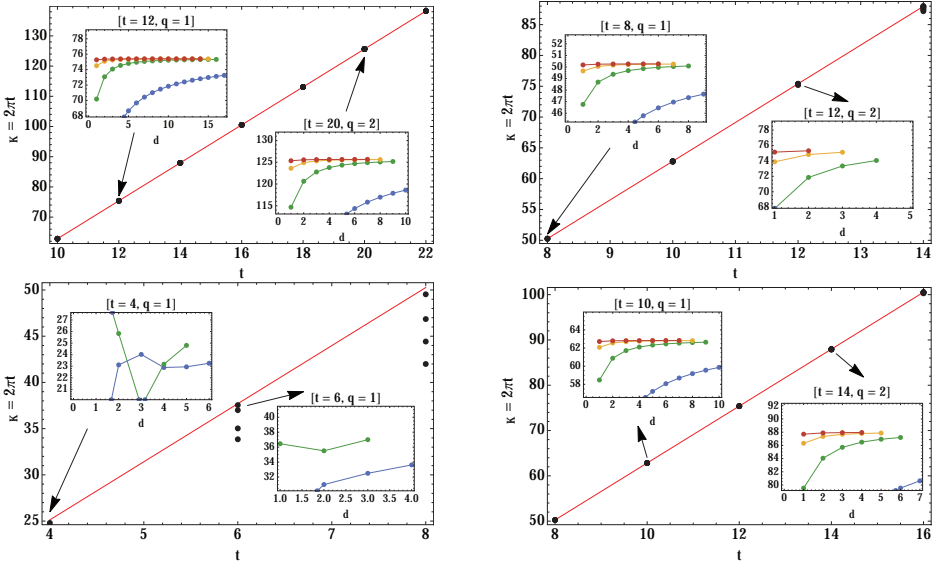


Figure 10. Tests of the instanton action $A_K = 2\pi t$, from the Kähler saddle-point, for local \mathbb{P}^2 , ABJM, the quintic, and the local curve X_3 (from left to right and top to bottom). The inclosed plots show the convergence for a couple of values of t and q . Note that for the quintic we do not have enough data to guarantee reaching a limit where all black dots overlap.

The polynomials $\mathcal{P}_h(q)$ are precisely the *same* as in (3.47), and the integer q is introduced to make both g and d integer; see the discussion around equation (3.39).

Computational tests on the validity of (4.71) are shown in Figures 10 and 11; with Figure 10 testing the Kähler instanton action and Figure 11 testing the (universal) validity of the polynomials $\mathcal{P}_h(q)$ for $h = 0$ through 5. The precise nature of these computational tests is exactly the same as we did earlier for the resolved conifold, and we refer to that discussion for further details.

This formula (4.71), when restricted to the first approximation $h = 0$, reproduces the prediction from the saddle-point approximation which was explained around equation (2.30) (and leading up to it). Indeed, for the case of Kähler leading degree, $a_0 = -3/t$, $a_1 = 2/t$, $a_2 = t$, and $F_0^{(1)} = \frac{3A_K}{2\pi^2}$. Using these values in equation (2.30) (with $\beta = 1$) we precisely reproduce (4.71) truncated to $h = 0$. A numerical check of the values of a_0 and a_1 is

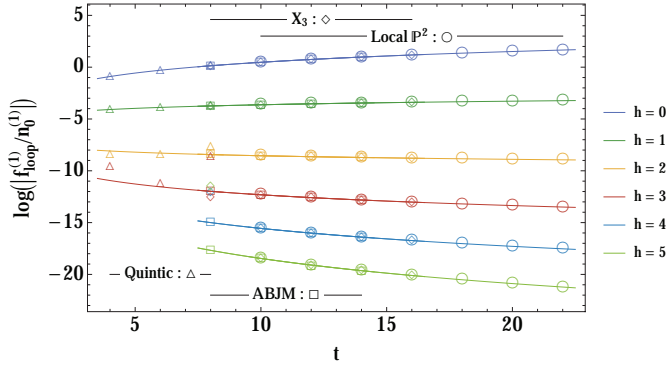


Figure 11. Numerical checks of the loop-corrections $f_h^{(1)} = \frac{n_0^{(1)} t^{\frac{3}{2}-h}}{2^{2h+1} \pi^{h+2}} \mathcal{P}_h(q)$, for $h = 0, \dots, 5$ and $q = 1$, for our several examples. We plot the logarithm of the ratio $f_0^{(1)}/n_0^{(1)}$ to have universal quantities which all fit within the same graph.

shown in the upper plots of Figure 12, for which we can nicely fit

$$(4.72) \quad a_0(Q)^{-1} = (-0.65 \pm 0.09) + (-0.274 \pm 0.008) t, \quad r^2 = 0.945,$$

$$(4.73) \quad a_1(Q)^{-1} = (0.038 \pm 0.005) + (0.4967 \pm 0.0004) t, \quad r^2 = 0.99995.$$

The shift in $a_0(Q)$ is not very reliable, but the slope in a_1 is quite close to the expected value.

This asymptotics arises from the $a_{d=1}$ contribution in the abc -expansion of the GW invariants in (2.20). Since $a_{d=1} = n_0^{(1)}$ one will always find the resolved-conifold asymptotics multiplied by this factor.

Conifold leading degree. The second dominant degree, $d = a_0(Q) + a_1(Q)g$, is harder to analyze as everything must now be approached numerically; from the computation of $a_0(Q)$ and $a_1(Q)$ to the asymptotics.

The numerical fit to $1/a_1(Q)$ is shown in the lower-right plot of Figure 12. It is obtained from first fitting straight lines $d = \alpha g + \beta$ for different (fixed) values of t . Then fitting these results against a linear dependence in t we have obtained

$$(4.74) \quad a_1(Q)^{-1} = (-0.466 \pm 0.005) + (0.2728 \pm 0.0005) t, \quad r^2 = 0.9998.$$

On what concerns $a_0(Q)$, its numerical calculation is shown in the lower-left plot of Figure 12, but there is no obvious fit to do here (numerically,

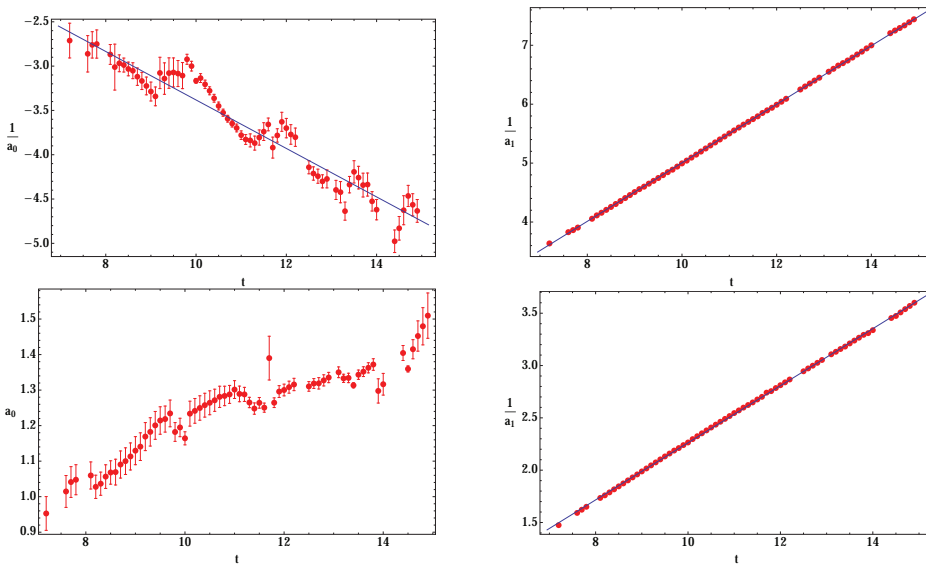


Figure 12. Local \mathbb{P}^2 : Numerical calculation of $a_0(Q)$ and $a_1(Q)$ associated to the Kähler instanton action (the two upper plots) and to the conifold instanton action (the two lower plots). We are showing tests for their inverses whenever the dependence seems linear, although we were not able to confirm this analytically in the case of the conifold action. (We are only plotting reasonably trustworthy fits, thus the apparent holes in the plots.)

the dependence of $1/a_0(Q)$ does not seem to be linear in t , yielding a poor $r^2 = 0.849$, and this will become even more evident in following examples). At this moment we cannot provide an analytical interpretation for these numbers, or even guarantee that the fit to a straight line is justified since the interval in t we have considered might be too small to be significant. Nonetheless, we do report the results.

Because we now lack the precision we had along the Kähler leading degree, we cannot provide a systematic exploration of the GW asymptotics with conifold leading degree. We can, however, identify particular values of t for which the exploration becomes simpler. One such point is found when $a_1(Q) = 1$, or $t \approx 5.6993\dots$. In this case we explore the growth of $N_{g,g+\Delta}$ for some integer $\Delta \in \mathbb{Z}$ (implicitly associated to $a_0(Q)$). The numerical exploration of this diagonal slice in the GW-table yields the result

$$(4.75) \quad N_{g,g+\Delta}^{\mathbb{P}^2} \sim \frac{\Gamma\left(2g - \frac{3}{2}\right)}{A_0^{2g - \frac{3}{2}}} e^{\alpha_0 + \alpha_1 \Delta} (-1)^{\Delta+1},$$

where $A_0 \approx 0.655995\dots$, and α_0 and α_1 are pure numbers which cannot be computed with much precision. The interesting point is that the value of A_0 can be matched to the saddle-point prediction involving the *conifold* action,

$$(4.76) \quad A_1(Q) \sqrt{Q} = 0.655995043\dots,$$

where the \sqrt{Q} comes from including the factor Q^d that multiplies $N_{g,g+\Delta}^{\mathbb{P}^2}$ in the saddle-point expression. On the other hand, the one-loop coefficient in (4.75) should correspond to

$$(4.77) \quad \left(\frac{a_2}{\pi a_1 A_1} \right)^{1/2} F_0^{(1)[c]},$$

but $a_2(Q)$ is directly related to the second derivative at the saddle point and thus it cannot be computed from first principles.

4.2. The example of local $\mathbb{P}^1 \times \mathbb{P}^1$

Let us next address another (toric) local surface, the non-compact CY threefold known as local $\mathbb{P}^1 \times \mathbb{P}^1$, which is the total space of the line bundle $\mathcal{O}(-2, -2) \rightarrow \mathbb{P}^1 \times \mathbb{P}^1$. Generically, local $\mathbb{P}^1 \times \mathbb{P}^1$ has two complex structure moduli, z_1 and z_2 , implying that the mirror map is similarly twofold, $Q_1 = e^{-t_1} = \mathcal{O}(z_1)$ and $Q_2 = e^{-t_2} = \mathcal{O}(z_2)$. In order to have reasonable large-order data for the resurgence analysis, in what follows we shall restrict to a slice of this variety where $z_1 = z_2$.

Free energies and Gromov–Witten invariants. Instead of working in the full two-dimensional moduli space, we shall restrict to the (simpler) one-dimensional *diagonal slice* where the sizes of both \mathbb{P}^1 's in the local $\mathbb{P}^1 \times \mathbb{P}^1$ geometry are set to be *equal*. One is thus left with a single modulus. The resulting such theory is closely related to a rather well-known gauge theory, called ABJM gauge theory [61] (see also [62]), and we shall use this name in the following to denote this diagonal slice of local $\mathbb{P}^1 \times \mathbb{P}^1$.

Of course the general local $\mathbb{P}^1 \times \mathbb{P}^1$ geometry has two Picard–Fuchs operators; annihilating periods. One immediate simplification of the diagonal slice is to reduce this number to just one,

$$(4.78) \quad \left\{ (z\partial_z)^4 - 4z \left(4(z\partial_z)^3 + 4(z\partial_z)^2 + z\partial_z \right) \right\} f(z) = 0.$$

From its solutions, we can identify the mirror map and the genus-zero free energy,

$$(4.79) \quad -t = \log z + 4z + 18z^2 + \frac{400}{3}z^3 + \dots = \log Q,$$

$$(4.80) \quad F_0^{(0)} = c_3 t^3 + c_2 t^2 + c_1 t - 4Q - \frac{9}{2}Q^2 - \frac{328}{27}Q^3 + \dots$$

After dealing with the genus-one free energy, $F_1^{(0)}$, one can proceed and use the holomorphic anomaly equations to compute higher-genus free energies¹¹, from which the GW invariants are eventually read. For example, in the language of modular forms,

$$(4.81) \quad F_2^{(0)} = \frac{5E_2^3}{5184cd^2} - \frac{E_2^2}{576d^2} + \frac{E_2(c^2 - cd + d^2)}{864cd^2} \\ + \frac{-16c^3 + 15c^2d - 21cd^2 + 2d^3}{51840cd^2} \\ = -\frac{Q}{60} - \frac{Q^2}{20} - \frac{Q^3}{10} + \dots,$$

where $E_2(\tau)$ is the second Eisenstein series, $c = \vartheta_3^4(\tau)$ and $d = \vartheta_4^4(\tau)$ are powers of theta functions, and the modular parameter τ is a function of z ; see [63] for full details. Also, in this language $F_1^{(0)} = \log \eta(\tau)$ with $\eta(\tau)$ the Dedekind eta-function. In Appendix B.2 we list the first few GW invariants, and Figure 13 schematically represents the ones we have computed and will work with.

The instanton actions for ABJM were extensively discussed in [27] and are associated to special points in moduli space: large Kähler structure ($z = \infty$) yielding $A_K = 2\pi t$, conifold point ($z = z_c$) yielding A_c , and orbifold point ($z = 0$) yielding A_o . These three actions are actually *linearly dependent* with integer coefficients. This implies that the ABJM transseries (whose construction is still an open problem for future research) might either involve only two of these actions (selected upon some criteria of relevance), or it might involve all three of them (in which case one would obtain a resonant transseries as in, e.g., [28, 29, 38]).

¹¹This was done in [57] using the language of propagators, and addressing the full local $\mathbb{P}^1 \times \mathbb{P}^1$ geometry; and in [63] using modular forms, and while restricting to the ABJM diagonal slice.

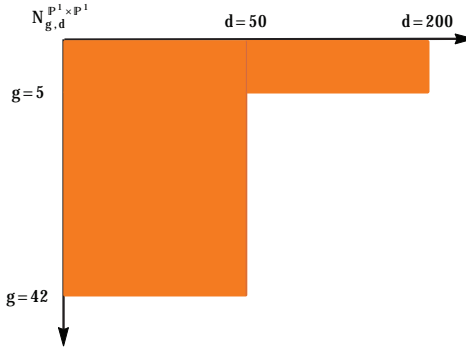


Figure 13. Maximum degree and genus of the GW invariants we computed for ABJM.

Analysis of large-degree growth. The large degree, fixed genus, growth is completely analogous to that of local \mathbb{P}^2 ,

$$(4.82) \quad N_{g,d} \sim c_g d^{2g-3} e^{dt_c} (\log d)^\delta.$$

The value of the Kähler parameter at the conifold point is now $t_c := t(z = 1/16) = 8K/\pi = 2.33248723\dots$ [63], where $K = \sum_{n=0}^{+\infty} (-1)^n (2n+1)^{-2}$ is the Catalan constant. The exponent δ numerically matches to the expected $2g - 2$. This g -dependence of the exponents may be tested using the same large- d sequences as for local \mathbb{P}^2 , *i.e.*, the combinations (4.61) and (4.62). These numerical results are illustrated in Figures 14, 15 and 16.

Analysis of large-genus growth. Again, the strategy is essentially the same as for the example of local \mathbb{P}^2 . As before, the GW invariants can be expanded in terms of *abc*-coefficients according to equation (2.20), but where in the present example one explicitly has $G_{\text{ABJM}}(d) = \lfloor d(d-4)/4 \rfloor + 1$. A table with these first few coefficients is shown in Appendix B.2.

The first few coefficients seem to answer to the closed-form formula

$$(4.83) \quad b_{d, \lfloor \frac{d(d-4)}{4} \rfloor - k}^{\text{ABJM}} = p_{d,-4}(k) 4d \left(\left\lfloor \frac{(d+2)^2}{4} \right\rfloor - k \right),$$

where

$$(4.84) \quad p_{d,-4}(k) = \begin{cases} p_{e,-4}(k)/2 & \text{even } d, \\ p_{o,-4}(k) & \text{odd } d, \end{cases}$$

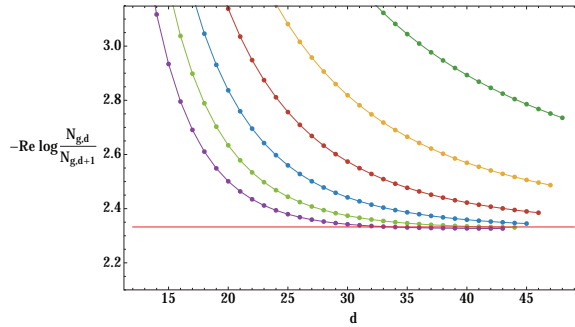


Figure 14. ABJM: The exponent t_c in the growth of $N_{g,d}$ is captured from the ratio of two consecutive GW invariants, when the degree is large. We plot that ratio alongside six Richardson extrapolations, which are clearly converging faster towards the expected result (up to a numerical relative error of about 0.3%).

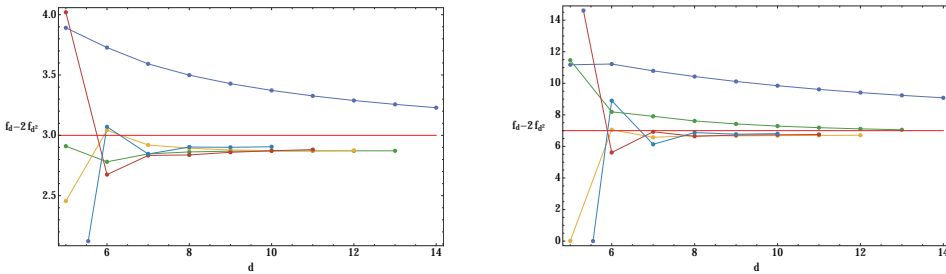


Figure 15. ABJM: The exponent $2g - 3$ is the leading large-order term in $f_d - 2f_{d^2}$. We have data up to $d = 200$ so that the horizontal axis can only reach $d = 14$. The plots illustrate the first few Richardson transforms for $g = 3$ (left) and $g = 5$ (right), converging faster towards the expected result (up to numerical relative errors of about 3% in both cases).

and

$$(4.85) \quad \sum_{k=0}^{+\infty} p_{e,-4}(k) q^k \stackrel{?}{=} (1 + 2q + 2q^4) \prod_{m=1}^{+\infty} \frac{1}{(1 - q^m)^4},$$

$$(4.86) \quad \sum_{k=0}^{+\infty} p_{o,-4}(k) q^k \stackrel{?}{=} (1 + q^2 + q^6) \prod_{m=1}^{+\infty} \frac{1}{(1 - q^m)^4}.$$

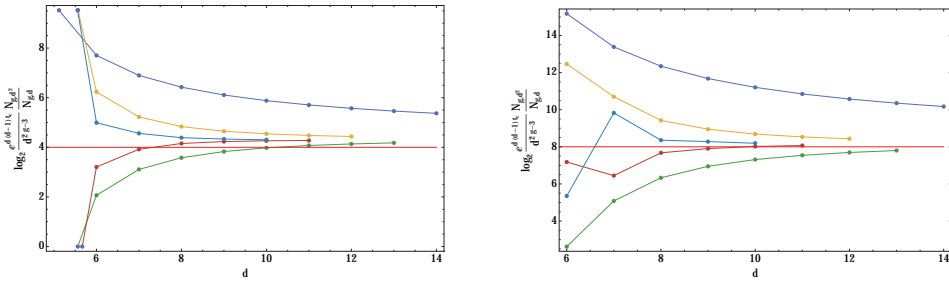


Figure 16. ABJM: The exponent δ of the logarithm $\log d$ is the leading term in the sequence (4.62). Having data up to $d = 200$ implies the horizontal axis only reaches $d = 14$. We plot the first few Richardson transforms for $g = 3$ (left) and $g = 5$ (right), converging faster towards the expected result (up to small numerical relative errors of about 8% and 3%, respectively).

But with the (limited) available data we cannot confirm that these formulae are complete.

Combined/diagonal large-growth in genus and degree. The combined growth in genus and degree is similar to the one for local \mathbb{P}^2 . The two leading combinations, again arising from Kähler and conifold instanton actions, will allow us to connect the factorial growth of the perturbative free energies with the factorial growth of GW invariants. This is illustrated in Figure 17. As already happened before, the growth associated to the Kähler action, $d = (2g - 3)/t$, is well understood since the example of the resolved conifold, whereas the one associated to the conifold action, $d = a_0(Q) + a_1(Q)g$, can only be probed numerically.

Kähler leading degree. This growth is completely determined, at least up to the first exponentially-subleading instanton corrections, by the first GV invariant of ABJM which in this case is $n_0^{(1)} = -4$. Thus we have

$$(4.87) \quad N_{g,d}^{\text{ABJM}} Q^d \Big|_{g=\frac{t}{2}d+q} \sim \sum_{h=0}^{+\infty} \frac{\Gamma(2g - \frac{3}{2} - h)}{A_K^{2g - \frac{3}{2} - h}} \frac{n_0^{(1)} t^{\frac{3}{2} - h}}{2^{2h+1} \pi^{h+2}} \mathcal{P}_h(q),$$

where $A_K = 2\pi t$ and the definition of $\mathcal{P}_h(q)$ is given in (3.47), *i.e.*, they are precisely the same polynomials which have already appeared for resolved conifold and local \mathbb{P}^2 . Computational tests on the validity of (4.87) are shown in Figures 10 and 11, with the exact same discussion as for resolved conifold and local \mathbb{P}^2 . In fact, all the very same comments we made for

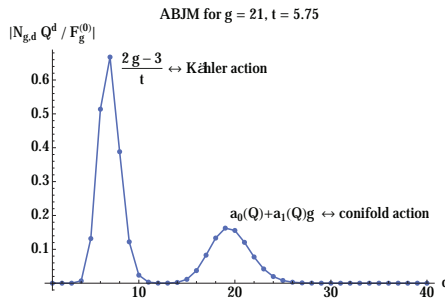


Figure 17. ABJM: Graphical representation of which GW invariants contribute the most to a free energy $F_g^{(0)}(Q)$, for fixed values of g and $Q = e^{-t}$. As for local \mathbb{P}^2 in Figure 3, ABJM has saddle points corresponding to both Kähler and conifold actions. The values of g and t in the plot were chosen as to clearly see both saddles in the same figure.

local \mathbb{P}^2 in Section 4.1 also apply now. In particular, the numerical check of $a_0 = -3/t$ and $a_1 = 2/t$ is indeed confirmed as

$$(4.88) \quad a_0(Q)^{-1} = (0.01 \pm 0.07) + (-0.33 \pm 0.01) t, \quad r^2 = 0.970,$$

$$(4.89) \quad a_1(Q)^{-1} = (-0.003 \pm 0.005) + (0.5000 \pm 0.0009) t, \quad r^2 = 0.99992.$$

This check is shown in the upper plots of Figure 18.

Conifold leading degree. In this case, the analysis can only be carried out numerically, due to lack of theoretical knowledge of where $a_0(Q)$ and $a_1(Q)$ come from. The strategy is essentially the one already started with local \mathbb{P}^2 , and we find

$$(4.90) \quad a_1(Q)^{-1} = (-0.595 \pm 0.009) + (0.307 \pm 0.002) t, \quad r^2 = 0.9993.$$

This fit is shown in the lower-right plot of Figure 18. The lower-left plot of this figure shows the numerical calculation of $a_0(Q)$, again with no obvious fit to do here.

4.3. The example of the local curve X_p

Our next example deals with local curves. The non-compact CY threefolds to be considered are the total spaces of the rank-two holomorphic vector bundles $X_p \simeq \mathcal{O}(p-2) \oplus \mathcal{O}(-p) \rightarrow \mathbb{P}^1$, with p an integer (but due to the invariance $p-2 \leftrightarrow -p$, one may choose $p \in \mathbb{N}$). When $p = 1$ one finds the

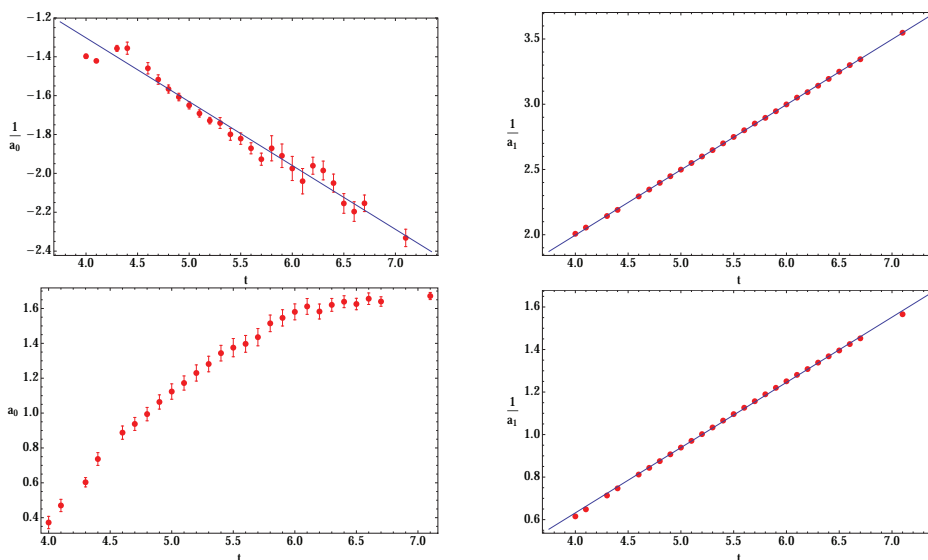


Figure 18. ABJM: Numerical calculation of $a_0(Q)$ and $a_1(Q)$ associated to the Kähler instanton action (the two upper plots) and to the conifold instanton action (the two lower plots). We are showing test for their inverses whenever the dependence seems linear, although we were not able to confirm this analytically in the case of the conifold action.

resolved conifold, $\mathcal{O}(-1) \oplus \mathcal{O}(-1) \rightarrow \mathbb{P}^1$ (addressed earlier), and when $p = 2$ one finds the Dijkgraaf–Vafa geometries $\mathcal{O}(0) \oplus \mathcal{O}(-2) \rightarrow \mathbb{P}^1$ relating to hermitian matrix models [64].

By making use of the topological vertex machinery [65] one may actually compute high genus GW invariants for the local curve directly in the A-model. We shall nonetheless begin with some comments pertaining to the B-model free energy, following [43].

Free energies and Gromov–Witten invariants. The B-model free energy has the general structure [43]

$$(4.91) \quad F_g^{X_p}(w) = \frac{1}{(w - w_c)^{5(g-1)}} \sum_{n=1}^{5(g-1)} a_{g,n}(p) (w - 1)^n,$$

where the coefficients $a_{g,n}$ are of the form

$$(4.92) \quad a_{g,n} = \frac{b_{g,n}(p)}{(p - 1)^k},$$

with k a positive integer and $b_{g,n}(p)$ a polynomial in p . They are not known in general and have to be fixed with GW invariants up to degree $d = 5(g - 1)$ (we present some of these coefficients in Appendix B.3). The modulus w is related to the Kähler parameter t through the mirror map

$$(4.93) \quad Q \equiv e^{-t} = w^{(p-1)^2-1} - w^{(p-1)^2},$$

where the critical point is at

$$(4.94) \quad w_c = \frac{p(p-2)}{(p-1)^2},$$

which translates to

$$(4.95) \quad t_c = \log \left((p(p-2))^{p(2-p)} (p-1)^{2(p-1)^2} \right).$$

It is interesting to notice that, unlike the previous geometries, all these formulae are now *exact*. Further notice that the double-scaled theory at the critical point is now in the universality class of 2d gravity (the free energy being related to the Painlevé I equation) which is a distinct universality class from the previous $c = 1$ examples [43].

As mentioned earlier, one can compute the partition function, and thus the free energy, as a sum over integer partitions directly in the A-model using the topological vertex [65]. We shall not get into any details, which may be found in [43], and simply quote the end results. We have computed¹² GW invariants $N_{g,d}^{X_p}$ with fixed $p = 3, 4, 5$ and in Appendix B.3 we list a few such invariants. Figure 19 schematically represents all the invariants we did compute and will work with herein. In the rest of this section we will mostly omit the p -dependence of the GW invariants for shortness, but our results for the different types of growth will always be for general p unless explicitly stated otherwise. We should also point out that we are including an extra

¹²On a technical aside, let us mention that the main obstacle in such A-model computations is the growth in degree, since it implies considering an exponentially-growing number of partitions and ever larger expressions to put together. The expansion of the free energy in powers of g_s is also time and resource-consuming, but this computation can be improved if we compute the GW invariants numerically. The only requisite is that the numerical precision should be high enough in order to extract rational numbers out of decimal expansions.

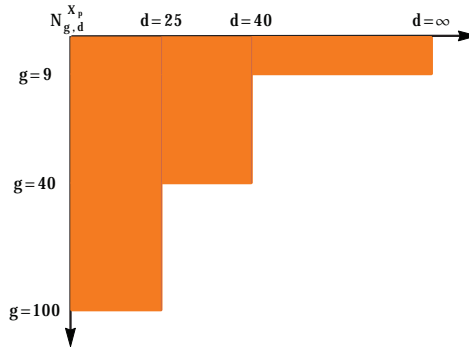


Figure 19. Maximum degree and genus of the GW invariants we computed for the local curves X_p with $p = 3, 4, 5$. For $g \leq 9$ we have all the required data to fix (4.91) and thus can compute GW invariants for any degree.

sign in our GW invariants [49, 50]

$$(4.96) \quad N_{g,d}^{X_p} \rightarrow (-1)^{g-1} N_{g,d}^{X_p}.$$

This is essentially required in order to produce integer GV invariants.

For $g \leq 9$ we have enough data to completely fix the coefficients in (4.91), which means the GW invariants can then be computed to arbitrarily high degree. It is also worth mentioning that for $g = 0, 1$ there are explicit formulae for the GW invariants [43]

$$(4.97) \quad N_{0,d}^{X_p}(p) = -\frac{(df - 1)!}{d! d^2 (d(f - 1))!},$$

$$(4.98) \quad N_{1,d}^{X_p}(p) = \frac{1}{24d} \sum_{n=0}^{d-1} \frac{f^{d-n}}{n!} \prod_{k=1}^n (d(f - 1) + k - 1) - \frac{1}{24 d!} \frac{(df - 1)!}{(d(f - 1))!} (f + 2),$$

where we have set $f \equiv (p - 1)^2$, and where higher-genus closed-form generalizations are not known. One general thing which is known [43] is that if written for arbitrary p , as $N_{g,d}^{X_p}(p)$, the GW invariants are polynomials of

degree $2g + 2d - 2$ in p , with rational coefficients,

$$(4.99) \quad N_{g,d}^{X_p}(p) = \sum_{n=0}^{2g+2d-2} N_{g,d,n} p^n.$$

Analysis of large-degree growth. The analysis of the fixed-genus, large-degree growth of GW invariants in this example is best achieved within the B-model formulation (4.91). The A-model (topological vertex) calculation is only efficient up to about degree $d = 40$ and, as we shall see, the large-degree convergence of the GW invariants is very slow. Using data up to genus $g = 40$ (for $p = 3, 4$) we have fixed the coefficients $a_{g,n}$ up to $g = 9$ and then can compute $N_{g \leq 9, d}$ up to very high degree.

To see how this works, rewrite (4.91) as

$$(4.100) \quad F_g^{X_p}(t) = \sum_{k=0}^{5(g-1)} \alpha_{g,k} (w - w_c)^{k-5(g-1)}$$

with $\alpha_{g,k} = \sum_{n=1}^{5(g-1)} \binom{n}{k} a_{g,n} (w_c - 1)^{n-k}.$

A Lagrange inversion turns (4.100) into a Q -expansion (related to w via the mirror map (4.93)), from where GW invariants are easily extracted. We will skip these details and refer the reader to Appendix A of [43] for the definition of Lagrange inversion as well as instructive examples. In the end, one finds the explicit result

$$(4.101) \quad N_{g,d}^{X_p} = \frac{(-1)^{d-1}}{d} \sum_{k=0}^{5(g-1)} \alpha_{g,k} (5(g-1) - k) f^{d+5(g-1)-k} P_{d-1}^{(u,v)} \left(\frac{f-2}{f} \right),$$

where

$$(4.102) \quad u = k - d - 5(g - 1), \quad v = d(f - 1) + 5(g - 1) - k,$$

and where the $P_n^{(a,b)}(z)$ are Jacobi polynomials. Finding the large-degree behavior of the GW invariants now reduces to the corresponding large-degree behavior of the Jacobi polynomials. We still had to approach this behavior numerically, essentially because the degree d appears in three different places. Furthermore, the aforementioned slow convergence of the GW invariants will be made clear in the following, as the large-degree expansion

turns out to be a power-series expansion in \sqrt{d} for which our standard techniques of Richardson extrapolation are not very useful. However, restricting the study to a grid of perfect squares, *i.e.*, $d = \ell^2$, we then get back the very fast convergence via Richardson transforms, from where one can then comfortably find rational numbers out of decimal expansions.

Consider the following combination

$$(4.103) \quad P_{d,g,k}(f) \equiv f^{d+5(g-1)-k} (5(g-1) - k) P_{d-1}^{(u,v)} \left(\frac{f-2}{f} \right),$$

for which we find a large-degree expansion of the form

$$(4.104) \quad P_{d,g,k}(f) = (-1)^{d-1} e^{dt_c} d^{\frac{5}{2}(g-1) - \frac{k}{2}} \sum_{n=0}^{+\infty} c_{g,k}^{(n)} d^{-\frac{n}{2}} \\ \simeq (-1)^{d-1} e^{dt_c} d^{\frac{5}{2}(g-1) - \frac{k}{2}} \left(c_{g,k}^{(0)} + \frac{c_{g,k}^{(1)}}{\sqrt{d}} + \dots \right).$$

Using $\widehat{g} \equiv 5(g-1)$ for shortness, the first coefficients are

$$(4.105) \quad c_{g,k}^{(0)} = \frac{e^{\frac{1}{2}(\widehat{g}-k)t_c} \mathcal{A}^{k-\widehat{g}}}{\Gamma\left(\frac{1}{2}(\widehat{g}-k)\right)}, \\ c_{g,k}^{(1)} = \frac{\sqrt{2}}{3} \frac{e^{\frac{1}{2}(\widehat{g}-k)t_c} \mathcal{A}^{k-\widehat{g}}}{\Gamma\left(\frac{1}{2}(\widehat{g}-k-1)\right)} \frac{f-2}{\sqrt{f(f-1)}} (\widehat{g}-k),$$

where we have defined

$$(4.106) \quad \mathcal{A} = \sqrt{2} \frac{w_c^{1-(p-1)^2/2}}{p-1}.$$

In general, they will have the structure

$$(4.107) \quad c_{g,k}^{(j)} = \frac{e^{\frac{1}{2}(\widehat{g}-k)t_c} \mathcal{A}^{k-\widehat{g}}}{\Gamma\left(\frac{1}{2}(\widehat{g}-k-j)\right)} \frac{1}{(f(f-1))^{\frac{j}{2}}} \sum_{j_0=1}^j \widehat{c}_{j_0}^{(j)}(f) (\widehat{g}-k)^{j_0},$$

with $\widehat{c}_{j_0}^{(j)}(f)$ a polynomial in f of degree j . We refer to Appendix B.3 for a few such explicit results at the lowest orders. From these results it immediately follows that the leading term in $P_{d,g,0}$ reproduces the known behavior of the GW invariants (2.11) (with $\alpha = \beta = 0$ and $\gamma = -1/2$), and the coefficients can be shown to match the solution of Painlevé I, in the appropriate

double-scaling limit. This leading behavior then has corrections, suppressed by powers of $d^{-1/2}$.

The GW invariants for arbitrary p (or f) thus have the following large-degree expansion¹³

$$\begin{aligned}
 (4.108) \quad N_{g,d} &\sim e^{dt_c} d^{\frac{5}{2}(g-1)-1} \left(c_{g,0}^{(0)} \alpha_{g,0} + \frac{c_{g,1}^{(0)} \alpha_{g,1} + c_{g,0}^{(1)} \alpha_{g,0}}{\sqrt{d}} + \dots \right) \\
 &= e^{dt_c} d^{\frac{5}{2}(g-1)-1} \sum_{j=0}^{+\infty} \sum_{j'=0}^{\text{Min}(j, 5(g-1))} c_{g,j'}^{(j-j')} \alpha_{g,j'} d^{-\frac{j}{2}}.
 \end{aligned}$$

This result is illustrated and tested in Figure 20. On its left plot we consider the ratio $N_{g,d}^{(\text{pred})}/N_{g,d}$, where the asymptotic prediction in the numerator consists of using the expansion (4.108) up to the subleading correction $j = 0$ (blue), $j = 2$ (green), $j = 4$ (yellow) and $j = 6$ (red), up to degree $d = 100$ and fixed genus $g = 3$. At degree $d = 100$ the leading-order term is of the right order of magnitude, but it is still off by about $\sim 75\%$. Upon inclusion of subleading terms, the ratio then starts approaching 1, faster and faster. On the right plot of Figure 20 we show the number of decimal places of agreement between the GW invariants and their large-degree expansion, with the same color coding. This time we move only along perfect squares and work with fixed genus $g = 6$. At $d = 10000$ the leading term is still only good enough for the first decimal place, but then the agreement improves significantly once we start adding subleading corrections.

Analysis of large-genus growth. As discussed earlier, the large-genus fixed-degree growth of the GW invariants may be read directly from the abc -formula (2.20). In the case of the local curve, it simply reads

$$(4.109) \quad N_{g,d}^{X_p} = f_g^{\text{coni}} \left\{ \sum_{n|d} a_n^{X_p} \left(\frac{d}{n} \right)^{2g-3} + \frac{2g}{B_{2g}} \frac{1}{d} \left(c_d^{X_p} \delta_{g,1} + \sum_{n=1}^{G_{X_p}(d)-1} b_{d,n}^{X_p} n^{2g-2} \right) \right\},$$

where now $G_{X_p}(d) = (d - 1)((p - 2)d - 2)/2$. A table with the first few abc -coefficients may be found in Appendix B.3. To show an example, let us write

¹³Note that one interesting feature of this $\gamma = -1/2$ universality class, and as compared to the general structure in (2.11), is that there are no logarithmic contributions to the large-degree asymptotics.

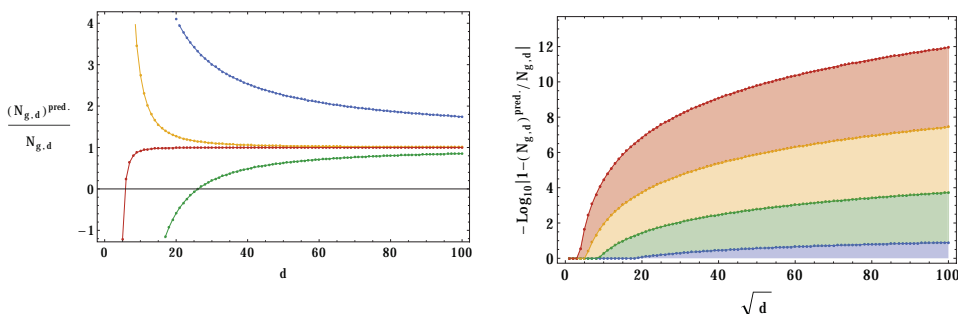


Figure 20. Local curve: Left: Comparison between $p = 3$ GW invariants and their asymptotic prediction in (4.108), at fixed genus $g = 3$ and degree $d \leq 100$, and up to subleading correction $j = 0$ (blue), $j = 2$ (green), $j = 4$ (yellow) and $j = 6$ (red). Right: Number of decimal places of agreement between the analytical $p = 3$ GW invariants and their asymptotic prediction, for fixed genus $g = 6$ (and using the same color code).

down the first couple of terms for $p = 3$

$$(4.110) \quad N_{g,d}^{X_3} \sim \frac{2(2g-1)}{d^3} \left(\frac{d}{2\pi}\right)^{2g} \left\{ 1 + (-1)^{d-1} 7^{\frac{1+(-1)^d}{2}} \frac{1}{2^{2g}} + 55^{(1+2d^2) \bmod 3} \frac{1}{3^{2g}} + \mathcal{O}(4^{-2g}) \right\}.$$

This expression is valid for any degree, unlike in previous examples.

Combined/diagonal large-growth in genus and degree. The combined “diagonal” growth will turn out to be similar to the previous local-surface examples (and in fact will lead to some sort of *large-order universality* for topological strings in different double-scaled universality classes). In fact, also in the local-curve case we cannot (analytically) pinpoint the nonperturbative structure of the GW invariants in a general situation where $d = a_0(Q) + a_1(Q)g$. As usual, the one exception happens at large-radius $t \rightarrow +\infty$, where the contribution of the GW invariants to the free energy is strongly peaked around $d = (2g - 3)/t$. These Kähler and critical-point peaks are illustrated in Figure 21.

The nonperturbative structure of the local-curve free-energy was addressed in [21, 22, 43], where instantons associated to spectral-curve B-cycles were found to control the large-order behavior of the free energy. But, as we shall see, as one moves towards larger and larger values of t this picture

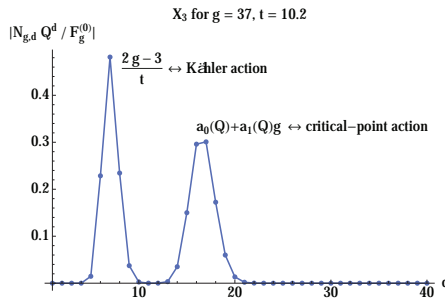


Figure 21. Local curve: Graphical representation of which GW invariants contribute the most to a free energy $F_g^{(0)}(Q)$, for fixed values of g and $Q = e^{-t}$, and with $p = 3$. As for the earlier examples of local \mathbb{P}^2 in Figure 3 and ABJM in Figure 17, also the local curve has saddle points corresponding to both Kähler and critical-point actions. The values of g and t in the plot were chosen as to clearly see both saddles in the same figure.

changes. Let us first address this question within the free energy itself, before translating to the GW invariants. For the remainder of this section we work with an approximated free energy

$$(4.111) \quad F_g^{X_p}(t) \approx (F^{X_p})_g^*(t) := \sum_{d=1}^{d_{\max}(g)} N_{g,d}^{X_p} e^{-dt},$$

where $d_{\max}(g)$ is the highest degree for which we have computed $N_{g,d}^{X_p}$ (our data is represented in Figure 19). We should stress that, with the leading contributions arising from near $d = \frac{2g-3}{t}$, we can always be sure that no significant contributions were left unaccounted for, and, in the end, the high accuracy of the large-order predictions will confirm that there are no issues with our approximation (4.111). What we find at large-order resembles the resolved conifold (3.35), in that the leading factorial growth is governed by a Gaussian-like action $A = 2\pi t$ with a one-instanton sector that truncates at two-loops¹⁴. In addition, there is a tower of other contributions that amounts to replacing the Kähler modulus t with $t_n = t + 2\pi i n$, $n \in \mathbb{Z}_{\neq 0}$, or,

¹⁴This is also true for all higher instanton sectors.

equivalently, with shifted instanton actions $A_n = A + 4\pi^2 i n$. The result is

$$(4.112) \quad F_g^{X_p}(t) \sim \frac{\Gamma(2g-1)}{\pi(2\pi t)^{2g-1}} \left(t + \frac{t}{2g-2} \right) + \sum_{m=1}^{+\infty} \frac{\Gamma(2g-1)}{\pi|A_m|^{2g-1}} \left\{ 2|t_m| \cos((2g-2)\theta_m) + \frac{2|t_m|}{2g-2} \cos((2g-2)\theta_m) \right\},$$

where we have also defined $\theta_m := \arg A_m = \arctan \frac{2\pi n}{t}$. It may be instructive to rewrite the above large-order relation in a more standard resurgence language, similar to (2.5). The difference is that now we have infinitely-many instanton actions A_m , where expansions around each sector truncate at two loops. In this way we rewrite (4.112) as

$$(4.113) \quad F_g^{X_p,(0)}(t) \sim \frac{S_1}{2\pi i} \sum_{m \in \mathbb{Z}} \frac{\Gamma(2g-1)}{A_m^{2g-1}} \left\{ F_{m,1}^{X_p,(1)}(t_m) + \frac{F_{m,2}^{X_p,(1)}(t_m) A_m}{2g-2} \right\} + 2\text{-instanton corrections.}$$

One immediately identifies the Stokes constant $S_1 = 2i$, and the one-instanton, one- and two-loop coefficients

$$(4.114) \quad F_{m,1}^{X_p,(1)}(t_m) = t_m, \quad F_{m,2}^{X_p,(1)}(t_m) = \frac{1}{2\pi}.$$

Tests of the large-order prediction (4.112) are shown in Figure 22, where it proves convenient to normalize the local-curve free energy against the Gaussian contribution, *i.e.*, we use $\mathcal{F}_g \equiv F_g - F_g^G$. The large-order growth of this normalized free-energy then corresponds to the second line in (4.112). In the left plot we show the normalized free energies for $t = 100$ (multiplied by an appropriate factor to make all numbers of $\mathcal{O}(1)$; the gray dots), alongside the sum in (4.112) up to $m = 2$ (green), $m = 4$ (yellow) and $m = 6$ (red). One can clearly see that the agreement with the data gets better and better by including more terms in the tower of corrections in (4.112). In the right plot we further illustrate this by showing how small the error is for $t = 24$. We use the normalized free-energy and define the error as $\left| 1 - \mathcal{F}_g^{\text{pred},m} / \mathcal{F}_g^{(0)} \right|$, where $\mathcal{F}_g^{\text{pred},m}$ just corresponds to taking the second line of (4.112) up to a given maximum (the colors are the same as the ones used on the left). We see that for $m = 6$, at $g = 100$, the error is of the order $10^{-58}\%$.

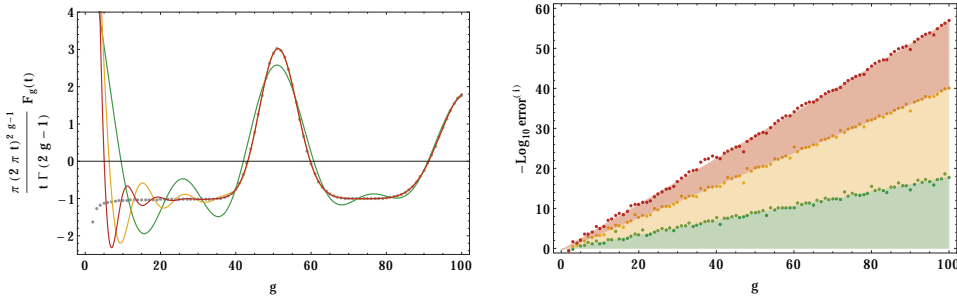


Figure 22. Local curve: Left: Comparison between the $p = 3$ free energy, with an appropriate pre-factor (the gray dots), and the predictions coming from (4.112) up to $m = 2$ (green), $m = 4$ (yellow) and $m = 6$ (red); showing a quicker convergence the more terms are included. Right: Logarithm of the error in the predictions (with the same colors), this time against the normalized free energy. For $m = 6$, at genus $g = 100$, the error is roughly of the order of one part in 10^{60} .

Let us comment on the relation to the large-order behavior found in [21, 22]. There should be a value of the Kähler parameter for which there is an effective competition between the B-cycle action found in [21, 22] and the Gaussian-like tower described above. Unfortunately, our data does not allow us to directly look at this interplay, for as one moves towards smaller t the contribution to the free energies is no longer dominated just by the invariants close to $d = \frac{2g-3}{t}$. There will also be other relevant contributions at higher degree, which we do not have enough data to account for. Nonetheless, do notice that an exchange in large-order dominance should be precisely related to this emergence of relevant contributions beyond the large-radius “peak”.

Given the above large-order behavior of the free energy, we may next deduce its consequences towards the “diagonal” growth of GW invariants. After accounting for the appropriate Gaussian correction, it turns out that the GW large-order is of the exact same type as in earlier examples (in this case, $n_0^{(1)} = (-1)^{p-1}$),

$$(4.115) \quad N_{g,d}^{X_p} Q^d \Big|_{g=\frac{t}{2}d+q} \sim \sum_{h=0}^{+\infty} \frac{\Gamma(2g - \frac{3}{2} - h)}{(2\pi t)^{2g - \frac{3}{2} - h}} \frac{n_0^{(1)} t^{\frac{3}{2} - h}}{2^{2h+1} \pi^{h+2}} \mathcal{P}_h(q),$$

where the $\mathcal{P}_h(q)$ are precisely the polynomials which were introduced in (3.40), and which also appeared in the similar large-order results for local \mathbb{P}^2 and local $\mathbb{P}^1 \times \mathbb{P}^1$. Computational tests on the validity of this expression

are shown in Figures 10 and 11, with their details and discussion being the same as before. One thus finds that even for theories in different (critical) universality classes, there is some sort of *universal large-order behavior* taking place at large radius¹⁵. This is also very clear in the plots in Figures 10 and 11. Furthermore, in the case of the local curve X_p , this large-order behavior turns out to be *independent* of p (up to a sign).

4.4. The example of Hurwitz theory

Let us now address a slightly more algebraic example, that of Hurwitz theory. Generically, it addresses branched covers of algebraic curves, but herein we restrict to so-called *simple* Hurwitz numbers, denoted by $H_{g,d}^{\mathbb{P}^1}(1^d)$, which count the number of degree- d disconnected coverings of \mathbb{P}^1 by a genus- g Riemann surface. These numbers have a combinatorial definition in terms of Young tableaux, but — in line with what we have been doing — they also have a string-theoretic origin. Indeed, Hurwitz theory may be thought of as a topological string theory, as it can be obtained by a particular limit of the A-model on the local curve X_p [43]. This limit consists in taking

$$(4.116) \quad p \rightarrow +\infty, \quad t \rightarrow +\infty, \quad g_s \rightarrow 0,$$

while the combinations

$$(4.117) \quad g_H \equiv p g_s, \quad e^{-t_H} \equiv (-1)^p p^2 e^{-t},$$

are held fixed. A number of results can then be straightforwardly obtained by applying this limit to our results in the previous section.

Free energies and Gromov–Witten invariants. The Hurwitz free-energy was shown to satisfy a Toda-like equation in [67],

$$(4.118) \quad \exp \left\{ F^H(t_H - g_H) + F^H(t_H) + F^H(t_H + g_H) \right\} = g_H^2 e^{t_H} \partial_{t_H}^2 F^H(t_H).$$

However, regarding Hurwitz theory as a limiting local-curve in the sense explained above, implies one may compute the genus- g free energy directly

¹⁵It would be interesting to compare this to the B-model large-radius universality recently uncovered in [35, 66].

in the B-model as

$$(4.119) \quad F_g^{\text{H}} = \frac{1}{(1-\chi)^{5(g-1)}} \sum_{n=1}^{3g-3} a_{g,n}^{\text{H}} \chi^n.$$

Here, the new variable χ is related to the local-curve B-model modulus w as

$$(4.120) \quad w - 1 = -\frac{\chi}{p^2},$$

and in the Hurwitz limit the mirror map becomes

$$(4.121) \quad e^{-t_{\text{H}}} = \chi e^{-\chi}.$$

In (4.119) one needs to use the appropriate limit of the $a_{g,n}(p)$ coefficients from (4.91), defined as

$$(4.122) \quad a_{g,n}^{\text{H}} = \lim_{p \rightarrow +\infty} p^{8(g-1)-2n} (-1)^n a_{g,n}.$$

From explicit results in Appendix B.3 one can see that only some of the coefficients contribute in the limit. The coefficients $a_{g,n}^{\text{H}}$ also turn out to be related to the perturbative free energies of 2d gravity as, under the appropriate double-scaling limit, the difference equation (4.118) reduces to the Painlevé I equation. A large-order analysis of the Hurwitz free energy was performed in [22] finding that large-order effects were, as expected, governed by the $p \rightarrow +\infty$ limit of the B-cycle instanton-action that controlled the large-order effects of the local curve.

In the A-model formulation, GW invariants are defined as usual. Furthermore, without surprise, they may also be obtained from the limit

$$(4.123) \quad N_{g,d}^{\text{H}} = \frac{H_{g,d}^{\mathbb{P}^1}(1^d)^{\bullet}}{(2g+2d-2)!} = \lim_{p \rightarrow +\infty} p^{2-2g-2d} N_{g,d}^{X_p}.$$

Here we have written the GW invariants in terms of *connected*, simple Hurwitz numbers $H_{g,d}^{\mathbb{P}^1}(1^d)^{\bullet}$. In practice, we computed the $N_{g,d}^{\text{H}}$ along the same lines as we computed the $N_{g,d}^{X_p}$, *i.e.*, starting from the partition function, then computing the free energy at fixed degree, and finally expanding in powers of g_{H} . We have computed (4.123) up to the totals schematically shown in Figure 23 (also see Appendix B.4). For $g \leq 17$, data up to $d = 50$ is enough to fix all the coefficients in (4.119), and we may thus compute GW invariants for any degree. This data will not be crucial in the following, since several

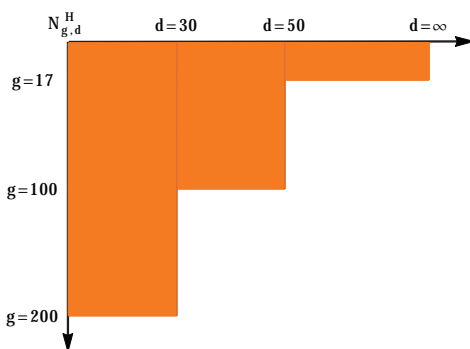


Figure 23. Maximum degree and genus of the GW invariants we computed for Hurwitz theory. These are related to simple Hurwitz numbers via (4.123). For $g \leq 17$ we have all the required data to fix (4.119) and thus can compute GW invariants for any degree.

results just follow from the “finite p ” case addressed before. Nonetheless, the ability to generate more data also allows us to make predictions to higher orders.

Analysis of large-degree growth. The asymptotic¹⁶ growth of Hurwitz numbers at large degree d , with fixed genus, may be extracted from what we found earlier for the local curve. In particular, one can apply the limit (4.123) directly to (4.108), so that after introducing¹⁷

$$\begin{aligned}
 \widehat{c}_{g,k}^{(j)} &= \frac{2^{\frac{1}{2}(k-5(g-1))}}{\Gamma\left(\frac{1}{2}(5(g-1)-k-j)\right)} \sum_{j_0=1}^j \widehat{c}_{j_0}^{\text{H},(j)} (5(g-1)-k)^{j_0}, \\
 \widehat{c}_{j_0}^{\text{H},(j)} &= \lim_{f \rightarrow +\infty} \frac{\widehat{c}_{j_0}^{(j)}(f)}{(f(f-1))^{\frac{j}{2}}}, \quad \alpha_{g,k}^{\text{H}} = \lim_{f \rightarrow +\infty} f^{4(g-1)-k} \alpha_{g,k}(f),
 \end{aligned}
 \tag{4.124}$$

¹⁶Reference [68] also studies asymptotics of Hurwitz numbers $H_{g,\mu}$, with μ a partition with ℓ parts μ_1, \dots, μ_ℓ . However, the asymptotics considered in [68] are in the limit $\lim_{N \rightarrow +\infty} H_{g,N\mu}$. This is conceptually different from our large-degree expansion of simple Hurwitz numbers: our case corresponds to a partition $(1, \dots, 1)$ with d entries (the number which is growing), while in the results of [68] the length of the partition is always kept fixed.

¹⁷In this limit we can equally take $f \sim p^2 \rightarrow +\infty$.

we immediately arrive at

$$(4.125) \quad N_{\mathbf{g},d}^{\text{H}} \sim e^d d^{\frac{5}{2}(\mathbf{g}-1)-1} \sum_{j=0}^{+\infty} \sum_{j'=0}^{\text{Min}(j, 3(\mathbf{g}-1))} \tilde{c}_{\mathbf{g},j'}^{(j-j')} \alpha_{\mathbf{g},j'}^{\text{H}} d^{-\frac{j}{2}}.$$

Another route to this result would be to directly write GW invariants for Hurwitz theory, as we did in (4.101) for the local curve (one would now have to use the Hurwitz mirror map (4.121)). In this case, one obtains the GW invariants as¹⁸

$$(4.126) \quad N_{\mathbf{g},d}^{\text{H}} = \frac{(-1)^d}{d} \sum_{k=0}^{3\mathbf{g}-3} \alpha_{\mathbf{g},k}^{\text{H}} (5(\mathbf{g}-1) - k) L_{d-1}^{k-d-5(\mathbf{g}-1)}(d),$$

where the $L_m^a(z)$ are the associated Laguerre polynomials. Since the sum in (4.126) now runs over fewer values, it becomes easier to fix the necessary coefficients and generate GW invariants to arbitrarily large degree. Associated to the fact that the coefficients $\tilde{c}_{\mathbf{g},k}^{(j)}$ no longer depend on an extra parameter, we can find the large-degree expansion (4.125) to very high order with little effort. We present some of these results in Appendix B.4.

Analysis of large-genus growth. Hurwitz theory does not have an *abc*-formula, because the would-be GV invariants are no longer integers. Nonetheless, one can proceed empirically, using numerics and Richardson extrapolation, in order to find the growth of Hurwitz numbers for large genus, while at fixed degree. At low degree, the large-genus expansions actually *truncate*. For instance, for $d = 2, 3, 4$ we find

$$(4.127) \quad H_{g,2}^{\mathbb{P}^1} \left(1^d\right)^{\bullet} = \frac{1}{2},$$

$$(4.128) \quad H_{g,3}^{\mathbb{P}^1} \left(1^d\right)^{\bullet} = \frac{3^{2g-2}}{2},$$

$$(4.129) \quad H_{g,4}^{\mathbb{P}^1} \left(1^d\right)^{\bullet} = \frac{1}{2} (2^{2g+2} - 1) (3^{2g+4} - 1).$$

¹⁸We use the $\alpha_{\mathbf{g},k}^{\text{H}}$ coefficients for convenience; they are related to the $a_{\mathbf{g},i}^{\text{H}}$ in (4.122) via $(-1)^k \alpha_{\mathbf{g},k}^{\text{H}} = \sum_{i=1}^{3\mathbf{g}-3} \binom{i}{k} a_{\mathbf{g},i}^{\text{H}}$. They could just as well be fixed by using the mirror map and the Toda equation (4.118).

That is no longer the case for degree $d \geq 5$, where we now find

$$\begin{aligned}
 (4.130) \quad H_{g,d}^{\mathbb{P}^1} \left(1^d\right)^{\bullet} &= \frac{2}{(d!)^2} \left(\frac{d(d-1)}{2}\right)^{2d+2g-2} \\
 &\quad - \frac{2}{((d-1)!)^2} \left(\frac{(d-1)(d-2)}{2}\right)^{2d+2g-2} \\
 &\quad + \frac{2}{d^2 ((d-2)!)^2} \left(\frac{d(d-3)}{2}\right)^{2d+2g-2} \\
 &\quad - \frac{1}{2 ((d-2)!)^2} \left(\frac{(d^2-5d+8)}{2}\right)^{2d+2g-2} + \dots
 \end{aligned}$$

These results can also be easily derived by computing the free energy directly for low degree. For the purpose of illustration, let us show how the agreement between the exact $H_{g,d}^{\mathbb{P}^1} \left(1^d\right)^{\bullet}$ (for $d = 6$ and $g = 100$) and its prediction from (4.130) improves, as we include more terms. Note that this is an integer number with 241 digits, but we only display the first 82. One has:

$$\begin{aligned}
 H_{100,6}^{\mathbb{P}^1} \left(1^d\right)^{\bullet} &= 36773029021136586120108822348086934417891861531447353197011119061184878815704795302\dots \\
 \text{1-term} &= 36773029021136586120108822348086934556780750396609834115336352765962460171085765176\dots \\
 \text{2-terms} &= 36773029021136586120108822348086934417891861507720945226447463877073571282196876287\dots \\
 \text{3-terms} &= 36773029021136586120108822348086934417891861531447353197011119061187444102489809778\dots \\
 \text{4-terms} &= 36773029021136586120108822348086934417891861531447353197011119061184878815704795232\dots
 \end{aligned}$$

Combined/diagonal large-growth in genus and degree. Uncovering the combined growth in genus and degree for Hurwitz theory is a harder problem than in previous examples. The main reason being that in this example the “large-radius peak”, where GW invariants near $d = (2g - 3)/t$ give the main contribution to the free energy, no longer seems to exist. We did still numerically find another “critical-point peak”, as shown in Figure 24, but with the data we have available we were not able to find a linear relation, nor to uncover what the large-order behavior should be, analytically.

4.5. The example of the compact quintic

For our final example, we shall consider a compact geometry, in comparison to the non-compact local geometries we have been addressing up to now. This is actually the first example in which mirror symmetry was explicitly worked out and GW invariants systematically computed [4], the quintic CY

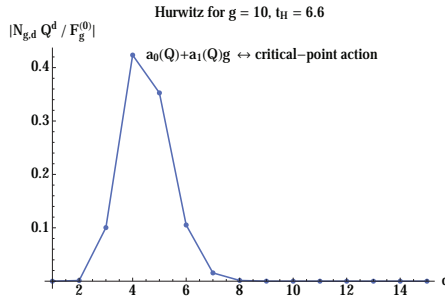


Figure 24. Hurwitz: Graphical representation of which GW invariants contribute the most to a free energy $F_g^{(0)}(Q)$, for fixed values of g and $Q = e^{-t_H}$. This time around we find a single saddle-point seemingly corresponding to the critical-point action.

threefold. The mirror of the quintic is described by the equation

$$(4.131) \quad \sum_{i=1}^5 x_i^5 - \frac{1}{z} \prod_{i=1}^5 x_i = 0,$$

where z captures the complex structure of the CY manifold. We will follow the notation in [69].

Free energies and Gromov–Witten invariants. As there is a single modulus, there is also a single Picard–Fuchs equation for the periods of this geometry, namely

$$(4.132) \quad \left\{ (z\partial_z)^4 - 5z(5z\partial_z + 1)(5z\partial_z + 2)(5z\partial_z + 3)(5z\partial_z + 4) \right\} f(z) = 0.$$

From its solutions, we find the mirror map and the genus-zero free energy,

$$(4.133) \quad -t = \log z + 770z + 717825z^2 + \frac{3225308000}{3}z^3 + \dots \equiv \log Q,$$

$$(4.134) \quad F_0^{(0)} = c_3t^3 + c_2t^2 + c_1t + 2875Q + \frac{4876875}{8}Q^2 + \frac{8564575000}{27}Q^3 + \dots$$

Akin to what happened for the local geometries, here the higher-genus free energies can also be described in compact form in terms of a few generators (or propagators). Each of them has a holomorphic expansion around the

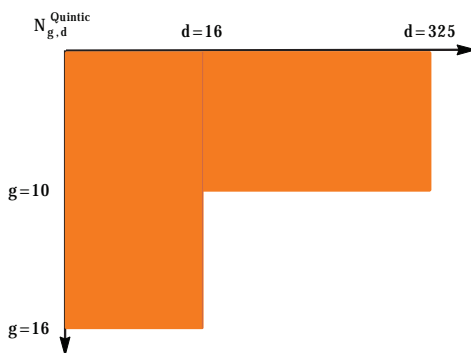


Figure 25. Maximum degree and genus of the GW invariants computed for the quintic.

large-radius point ($Q = 0$), from which one can read the GW invariants. For example,

$$(4.135) \quad F_2^{(0)} = \frac{575}{48}Q + \frac{5125}{2}Q^2 + \frac{7930375}{6}Q^3 + \dots$$

In this work we use the free energies which were computed in [69], and which are available online¹⁹. In Appendix B.5 we list a sample of the first GW invariants, and Figure 25 schematically represents the ones we used in our upcoming analysis. Note that we now have significantly less data than for the earlier non-compact examples, implying we will not have as many results.

Another important point is that there are essentially no studies of non-perturbative sectors for the quintic, mainly due to a lack of data to drive the analysis. However, it is natural to guess that there is an instanton action associated to the conifold point (located at $z = 5^{-5}$), $A_c = 2\pi T_c$, which is proportional to the flat coordinate T_c and vanishing at the conifold point. A test of this instanton action is shown in Figure 26, precisely confirming that this is indeed the case. We should also expect a Kähler instanton action, but we do not have enough free energies available to report definite results.

Analysis of large-degree growth. The large-degree growth at fixed genus was already considered in [6], being in the same universality class

¹⁹<http://uw.physics.wisc.edu/~strings/aklemm/highergenusedata/>

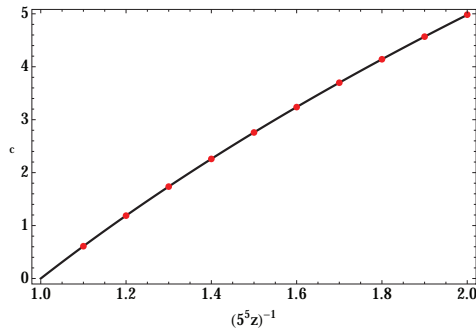


Figure 26. Quintic: Near the conifold point, the instanton action $A_c = 2\pi T_c$ controls the factorial growth of the free energies. In the figure we plot the analytic dependence of A_c against its numerical values computed from the large-genus growth of $F_g^{(0)}$, with a very clean match.

as local \mathbb{P}^2 or local $\mathbb{P}^1 \times \mathbb{P}^1$. In this case, the familiar asymptotic formula holds,

$$(4.136) \quad N_{g,d}^{\text{quint}} \sim c_g d^{2g-3} e^{dt_c} (\log d)^{2g-2},$$

where now $t_c := t(z = 5^{-5}) = 7.58995\dots$. One can numerically check the value of this critical exponent, t_c , as well as the powers in d^{2g-3} and $(\log d)^{2g-2}$, using the same asymptotic techniques described for local \mathbb{P}^2 and ABJM. We show these numerical results in Figures 27 and 28.

Analysis of large-genus growth. The fixed-degree, large-genus expansion of the GW invariants determines the *abc*-coefficients for the quintic in the same way it did for other geometries. In Appendix B.5 we present a sample of other such coefficients. Unfortunately, the scarce data available limits the analysis of the *b*-coefficients, and we have no other large-genus results to present for this example.

Combined/diagonal large-growth in genus and degree. As in previous examples, also for the quintic we find two saddle-points which are illustrated in Figure 29. They are associated to the Kähler instanton action, located at $d = (2g - 3)/t$, and to the conifold instanton action, located at $d = a_0(Q) + a_1(Q)g$, just like before.

Kähler leading degree. The scarce amount of available data does not let us check that the leading degree is $d = (2g - 3)/t$ in the same way as we did

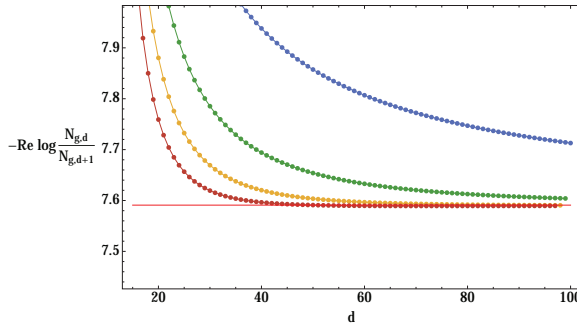


Figure 27. Quintic: The exponent t_c in the growth of $N_{g,d}$ is captured from the ratio of two consecutive GW invariants, when the degree is large. We plot that ratio alongside three Richardson extrapolations, which are clearly converging faster towards the expected result (up to a numerical relative error of about 0.2%).

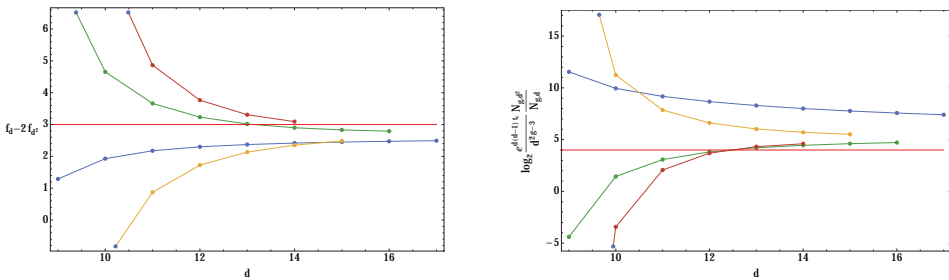


Figure 28. Quintic: On the left we address the exponent $2g - 3$, which is the leading large-order term in $f_d - 2f_d^2$. We have data up to $d = 325$ so that the horizontal axis can only reach $d = 17$. The plot illustrates the first few Richardson transforms for $g = 3$, converging faster towards the expected result (up to a numerical relative error of about 3%). On the right we address the exponent $2g - 2$ of the logarithm $\log d$, which is the leading term in the sequence (4.62). We plot the first few Richardson transforms for $g = 3$, converging faster towards the expected result (up to a numerical relative error of about 15%).

for local \mathbb{P}^2 or ABJM. Nevertheless, we can assume that this indeed holds, and then explore the asymptotics of $N_{g,d}^{\text{quint}} Q^d \Big|_{g=\frac{t}{2}d+q}$, just as we did in (4.71). We find that the same formula applies, but with the appropriate GV

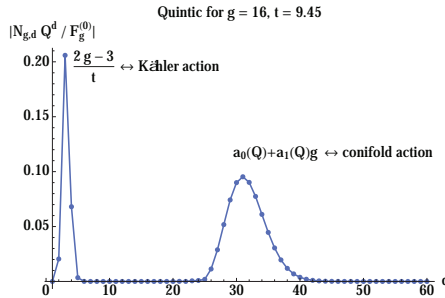


Figure 29. Quintic: Graphical representation of which GW invariants contribute the most to a free energy $F_g^{(0)}(Q)$, for fixed values of g and $Q = e^{-t}$. The values of g and t are carefully chosen so that both saddles are clearly visible in the same plot.

invariant $n_0^{(1)} = 2875$. Computational tests on the validity of such expression are shown in Figures 10 and 11, with their details and discussion being the exact same as before.

Conifold leading degree. For the conifold leading degree we can do better. Figure 30 shows the dependence of a_0 and a_1 upon the modulus t . The inverse of the slope, a_1^{-1} , resembles a straight line

$$(4.137) \quad a_1(Q)^{-1} = (-2.46 \pm 0.01) + (0.328 \pm 0.002) t, \quad r^2 = 0.9995.$$

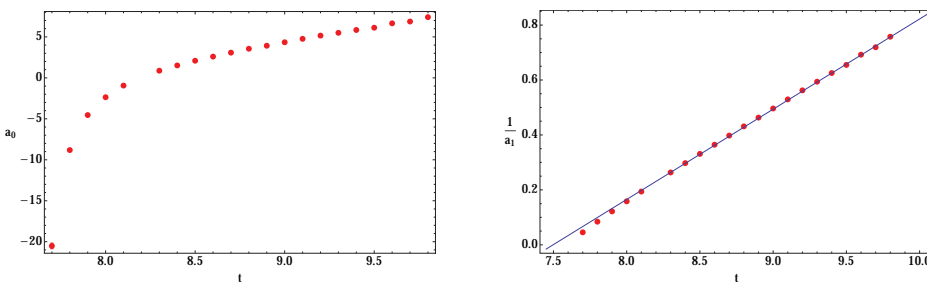


Figure 30. Quintic: Numerical calculation of $a_0(Q)$ and $a_1(Q)$ associated to the conifold instanton action. We show the inverse of a_1 because the dependence seems linear, although we are not able to confirm this analytically. The plot for a_0 does not seem to lead to any linear dependence.

Acknowledgments

We would like to thank Aleksey Zinger for discussions, and Marcos Mariño, José Mourão and João Pimentel Nunes for useful comments on the draft. RS would further like to thank the University of Geneva for extended hospitality, where a part of this work was conducted. RV would further like to thank the DESY Theory Group for support and hospitality. This research was partially supported by the FCT-Portugal grants EXCL/MAT-GEO/0222/2012, UID/MAT/04459/2013 and PTDC/MAT-GEO/3319/2014. The research of RS was partially supported by the Swiss-NSF grant NCCR 51NF40-141869 “The Mathematics of Physics” (SwissMAP).

Appendix A. Analysis of the *abc*-coefficients

When the GW invariants, $N_{g,d}$, may be written in terms of GV invariants, $n_g^{(d)}$, then there is a third representation in terms of some other integers we denoted by $a_d, b_{d,m}, c_d$. They appear naturally when considering the large-genus expansion of $N_{g,d}$.

Proposition A.1. *The relation between GW and GV invariants, and abc-coefficients is*

$$(A.1) \quad N_{g,d} = f_g^{coni} \left\{ \sum_{m|d} a_m \left(\frac{d}{m} \right)^{2g-3} + \frac{2g}{B_{2g}} \frac{1}{d} \left(c_d \delta_{g,1} + \sum_{m=1}^{G(d)-1} b_{d,m} m^{2g-2} \right) \right\},$$

$$(A.2) \quad a_d = n_0^{(d)},$$

$$(A.3) \quad b_{d,m} = \sum_{k|d,m} (-1)^{\frac{m}{k}} \frac{2d}{k} \sum_{h=\frac{m}{k}+1}^{G(\frac{d}{k})} n_h^{(\frac{d}{k})} \binom{2h-2}{h-1+\frac{m}{k}},$$

$$(A.4) \quad c_d = \sum_{m|d} m \left\{ n_1^{(m)} + 2 \sum_{h=2}^{G(m)} \frac{n_h^{(m)}}{h} \binom{2h-3}{h-2} \right\}.$$

Here $f_0^{coni} = 1$, $f_g^{coni} = (-1)^{g-1} \frac{B_{2g}}{2g(2g-2)!}$ for $g \geq 1$, and B_{2g} are the Bernoulli numbers. $G(d)$ satisfies $n_g^{(d)} = 0$ for $g > G(d)$. Since the GV invariants are integers, so are the abc-coefficients.

Proof. We start from the definition of GV invariants,

$$(A.5) \quad N_{g,d} = \sum_{h=0}^g c_{h,g} \sum_{m|d} n_h^{(m)} \left(\frac{d}{m}\right)^{2g-3} = \sum_{m|d} \sum_{h=0}^{G(m)} c_{h,g} n_h^{(m)} \left(\frac{d}{m}\right)^{2g-3},$$

where in the second equality we have noticed that $n_h^{(m)} = 0$ for $h > G(m)$. The coefficients $c_{h,g}$ generate $(2 \sin \frac{x}{2})^{2h-2} = \sum_{h=g}^{+\infty} c_{h,g} x^{2g-2}$, and they are explicitly given by

$$(A.6) \quad \begin{aligned} c_{0,g} &= f_g^{\text{coni}}, & c_{1,g} &= \delta_{g,1}, \\ c_{h,g} &= (-1)^{g-1} \frac{2}{(2g-2)!} \sum_{k=1}^{h-1} \binom{2h-2}{h-1+k} (-1)^k k^{2g-2}. \end{aligned}$$

Next, we organize the terms in (A.5) from more to less important as g grows, using (A.6). In order to do this, we split the h -sum in (A.5) into $h = 0$, $h = 1$, and $h \geq 2$. For $h \geq 2$ we can assume that also $g \geq 2$ and manipulate to arrive at (A.1). The steps are straightforward once one knows the goal, and they simply require the exchange of double sums, such as, *e.g.*, $\sum_{h=2}^{G(m)} \sum_{k=1}^{h-1} = \sum_{k=1}^{G(m)-1} \sum_{h=k+1}^{G(m)}$; or relabelings, such as, *e.g.*, $\sum_{m|d} f(m) = \sum_{m|d} f(d/m)$. The end result, after four of these manipulations, is

$$(A.7) \quad \begin{aligned} N_{g,d} &= f_g^{\text{coni}} \left\{ \sum_{m|d} n_0^{(m)} \left(\frac{d}{m}\right)^{2g-3} + \frac{2g}{B_{2g}} \frac{1}{d} \left(\delta_{g,1} \sum_{m|d} n_1^{(m)} m + \right. \right. \\ &\quad \left. \left. + \delta_{g \geq 2} \sum_{m=1}^{G(d)-1} \sum_{k|d,m} \sum_{h=\frac{m}{k}+1}^{G(\frac{d}{k})} n_h^{(\frac{d}{k})} \frac{2d}{k} \binom{2h-2}{h-1+\frac{m}{k}} (-1)^{\frac{m}{k}} m^{2g-2} \right) \right\}, \end{aligned}$$

from where one immediately can read the *abc*-coefficients. \square

We finish this appendix with a short note on how the GV and GW invariants, and the *abc*-coefficients, may be laid out in Dirichlet series for each genus g , in contrast to the usual Taylor-series expansion in the form of free energies. If we define the generating functions

$$(A.8) \quad \begin{aligned} \mathcal{GV}_g(s) &:= \sum_{d=1}^{+\infty} \frac{n_g^{(d)}}{d^s}, & \mathcal{GW}_g(s) &:= \sum_{d=1}^{+\infty} \frac{N_{g,d}}{d^s}, \\ \widetilde{\mathcal{GW}}_g(s) &:= \frac{\mathcal{GW}_g(s)}{\zeta(s - (2g - 3))}, \end{aligned}$$

then it follows from (A.5) the linear transformations

$$(A.9) \quad \widetilde{\mathcal{GW}}_g(s) = \sum_{h=0}^g c_{h,g} \mathcal{GV}_h(s) \quad \text{and} \quad \mathcal{GV}_g(s) = \sum_{h=0}^g \alpha_{g,h} \widetilde{\mathcal{GW}}_h(s).$$

Here, the α -coefficients arise from the generating function defined in [70],

$$(A.10) \quad \left(\frac{\arcsin(\sqrt{r}/2)}{\sqrt{r}/2} \right)^{2g-2} =: \sum_{h=0}^{+\infty} \alpha_{g+h,g} r^h.$$

We can also define Dirichlet series for the abc -coefficients, as

$$(A.11) \quad \mathcal{A}(s) := \sum_{d=1}^{+\infty} \frac{a_d}{d^s}, \quad \widehat{\mathcal{B}}_{2g-2}(s) := \frac{(-1)^{g-1}}{(2g-2)!} \frac{1}{\zeta(s-(2g-3))} \sum_{d=1}^{+\infty} \frac{b_{2g-2}(d)}{d^s},$$

where

$$(A.12) \quad b_{2g-2}(d) := \frac{1}{d} \left(c_d \delta_{g,1} + \sum_{n=1}^{G(d)-1} b_{d,n} n^{2g-2} \right).$$

They are linearly related to the previous Dirichlet series as

$$(A.13) \quad \begin{aligned} \widetilde{\mathcal{GW}}_g(s) &= f_g^{\text{coni}} \mathcal{A}(s) + \widehat{\mathcal{B}}_{2g-2}(s), & \mathcal{GV}_0(s) &= \mathcal{A}(s), \\ \mathcal{GV}_g(s) &= \sum_{h=1}^g \alpha_{g,h} \widehat{\mathcal{B}}_{2h-2}(s). \end{aligned}$$

The last expression can be inverted to define $\widehat{\mathcal{B}}_{2g-2}(s) = \sum_{h=1}^g c_{h,g} \mathcal{GV}_h(s)$.

Appendix B. Large-order enumerative data

B.1. Local \mathbb{P}^2

GW invariants

$\rho \setminus d$	1	2	3	4	5
0			244	12333	244328
1	$\frac{1}{2}$	-45	-23	3437	-43107
2	$\frac{1}{2}$	-36	-23	3437	-43107
3	$\frac{1}{2}$	0	30	514	43497
4	2016	336	30	1480	-1382717
5	37600	1920	1670	-500	38652363
6	1774080	14080	49280	22176	-633295419
7	3062644000	1320882400	1100765000	-1288228000	24205822400
8	2371249520000	280226856000	650326000000	3740016	-828592468107
9	1001788388674000	166525576874000	37848459272000	1588834044933	383492468107
10	108822274681100000	27613854692740000	562483492767000	33244469354933	-6804818406924139
11	2382209236364600000	31104185769461000	6467242844746307	46097042797496811	7038773488841801
12	245481768692693172300000	1487763826269316928000	681802424818476307	9583404248874465244	-383434948212924668273
13	40781809460865267474400000	3360387809269747280000	12092424658527650000	1823832463038077000	113662241587116966294000
14	8733217431824026528744000000	1455366874768219100341800600000	212684468074618159104600000	1461931436835482899000000	-51949882248874765841600000
15	142097655737831358598181813120000000	1683925746872310112818176000000	301374341139993691498246000000	2254643683636236884082208000000	1455366874768219100341800600000
16					48099185249539783274727104000000

$\rho \setminus d$	6	7	8	9
0	-102465	64639232	-110380263	6742682701
1	79922	-32624681	808703117	-18876568203
2	-1522743	42466957	-776658618	31156586249
3	34388102	-456595185	27816690931	-774029095237
4	21222927	364416184789	-31686667367	7262000066335821
5	5388569265	-1701382854615	6468894874407	-1194574000269297
6	-2410371757019	641306724810	-4310034250470053	921900472510784717
7	5406529415	-208388201280	6211277600040311	-771039468006446611
8	-24182305630333	12414311924618029271	-91929411676254000	280018871820972000
9	2927467884340002	-7109262886584706967	5282590437828934475267	-218807761668116630070274671
10	-96434782777629899	72974137618149808356483	-351563397698815428247468483	33371670015232037855045161439
11	20978819404347687	-133286967269708045274651	10018329644338105300926217	-10095224878222267477404930724199
12	-293889177657418974991	1467283687193397757695991095921	-429270511182688149394691726181	98762398901674092626964943693039
13	80842804974816416117	-2967097465243647041618262619	1819656900412650014344397204837	-9240949738925403463027282640326681
14	-1427287268168158244026123	17106929039444022034567341707903	-6927570053683633708883700079327607	22263736931301365324193096924707928687049
15	15381263971890314442000000	-21027676189833760764574880000301077	3988896562713683633269488000000000	-10648062507607613711768871000000
16	9076197263830343408479620000	430014724616459468686747490000	-819241304747676242925120000000	6688568010494811339388000000
	854483591692189976288747446000000	2088869511474666887479636362424000000	-61081074676946787466613620936000000	42103407467481618105408323541952491523000000

abc-coefficients

d	a_d^2	b_d^2	c_d^2	$n \setminus d$	4	5	6	7	8	9	10	11	12
1	3				336	-8 220	158 112	-2 852 178	50 177 472	-872 920 522	15 111 672 960	-261 287 923 314	4 519 291 217 184
2	-6				120	-3 960	95 364	-1 949 220	37 023 696	-678 641 328	12 204 852 900	-217 166 980 668	3 840 996 869 640
3	27				0	-1 710	54 672	-1 285 452	26 679 744	-518 992 740	9 736 728 480	-178 790 167 602	3 240 289 008 192
4	-192				0	-600	29 082	-819 000	18 795 464	-380 496 464	7 674 526 800	-145 852 020 072	2 135 908 064 644
5	1 695				0	-10	6 600	-297 360	8 704 224	-210 776 976	4 603 163 850	-94 464 959 688	1 862 891 778 168
6	-17 064				0	0	2 808	-168 420	5 716 608	-151 546 602	3 504 280 200	-75 031 171 842	1 527 561 613 296
7	188 454				0	0	972	-91 644	3 667 920	-106 820 532	2 637 683 220	-59 087 632 428	1 244 189 530 852
8	-2 228 160				0	0	336	-46 872	2 290 176	-74 248 344	1 963 227 240	-46 140 388 866	1 006 686 336 672
9	27 748 899				0	0	0	-22 848	1 394 016	-50 759 784	1 444 755 510	-35 729 687 796	809 231 436 144
10	-360 012 150				0	0	0	-4 284	821 952	-34 124 490	1 051 214 760	-27 438 015 792	646 325 964 576
11	4 827 935 987				0	0	0	171 024	-22 534 812	756 025 920	-20 895 548 256	512 927 354 016	4 898 553 006 800
12	-66 537 713 520				0	0	0	-504	137 904	-9 288 756	377 353 040	-11 816 321 368	316 915 489 680
13	988 273 463 465				0	0	0	0	691 200	-5 786 568	261 729 400	-8 773 420 590	246 780 346 080
14	-13 491 638 200 194				0	0	0	0	334 556	-3 522 204	179 174 760	-6 457 541 244	190 927 009 332
15	197 287 568 723 655				0	0	0	0	14 784	-2 095 956	121 053 360	-4 710 998 490	146 768 446 368
16	-2 927 443 754 647 296				0	0	0	0	6 192	-1 212 624	80 627 580	-3 405 917 196	112 094 549 136
					0	0	0	0	2 112	-682 830	52 935 600	-2 439 572 652	85 052 045 088
					0	0	0	0	720	-370 656	34 205 400	-1 730 850 132	64 106 083 800
					0	0	0	0	0	-194 922	21 753 000	-1 215 493 374	47 982 599 584
					0	0	0	0	0	56 400	-4 829 768	45 992 584	-97 180 000 000
					0	0	0	0	0	-46 818	8 332 680	-581 826 564	26 344 646 736
					0	0	0	0	0	-20 592	5 000 940	-395 979 804	19 311 539 496
					0	0	0	0	0	-8 586	2 940 480	-266 385 570	14 051 779 776
					0	0	0	0	0	-2 916	1 682 760	-177 075 888	10 147 793 400
					0	0	0	0	0	-990	939 600	-116 199 666	7 271 460 336
					0	0	0	0	0	506 220	506 220	-75 250 296	5 168 924 064
					0	0	0	0	0	265 200	265 200	-48 026 484	3 643 846 992
					0	0	0	0	0	157 200	157 200	-18 669 882	1 764 218 448
					0	0	0	0	0	63 240	63 240	-13 347 512	1 210 848 048
					0	0	0	0	0	27 720	27 720	-6 757 344	822 942 432
					0	0	0	0	0	11 520	11 520	-3 945 084	553 704 336
					0	0	0	0	0	3 900	3 900	-2 245 122	368 537 904
					0	0	0	0	0	1 320	1 320	-1 247 400	242 587 920
					0	0	0	0	0	0	0	-670 098	157 750 848
					0	0	0	0	0	0	0	-350 064	101 121 486
					0	0	0	0	0	0	0	-83 028	40 082 040
					0	0	0	0	0	0	0	-36 300	24 627 888
					0	0	0	0	0	0	0	-15 048	14 889 864
					0	0	0	0	0	0	0	-5 082	8 824 464
					0	0	0	0	0	0	0	-1 716	5 132 160
					0	0	0	0	0	0	0	0	2 910 672
					0	0	0	0	0	0	0	0	876 648
					0	0	0	0	0	0	0	0	450 840
					0	0	0	0	0	0	0	0	222 912
					0	0	0	0	0	0	0	0	106 488
					0	0	0	0	0	0	0	0	46 464
					0	0	0	0	0	0	0	0	19 224
					0	0	0	0	0	0	0	0	6 480
					0	0	0	0	0	0	0	0	2 184

d	a_d^2	b_d^2	c_d^2
1	3		
2	-6		
3	27		
4	-192		468
5	1 695		-7 560
6	-17 064		123 054
7	188 454		-2 014 488
8	-2 228 160		33 210 684
9	27 748 899		-551 883 810
10	-360 012 150		9 239 062 680
11	4 827 935 987		-155 687 687 496
12	-66 537 713 520		2 688 717 494 534
13	988 273 463 465		-44 952 069 548 178
14	-13 491 638 200 194		769 253 530 779 972
15	197 287 568 723 655		-13 217 019 911 660 760
16	-2 927 443 754 647 296		227 905 457 523 361 164

B.2. Local $\mathbb{P}^1 \times \mathbb{P}^1$

GW invariants

$d \setminus d$	1	2	3	4	5
0	-4	-2	-3/8	-7/7	-6/91
1	-3	-1/2	0	4	-1/25
2	-6	-1	0	4	4/85
3	-9	-3/2	0	-1/2	-3/2
4	-13/2	-1/8	-2/3	-1/8	8/39
5	-17/2	-1/10	-1/10	-8/9	-2/13
6	-19/2	-1/3	-7/30	-1/3	10/93
7	-20/2	-1/3	-2/3	-1/3	-2/17
8	-21/2	-1/3	-2/3	-1/3	2/17
9	-21/2	-1/3	-2/3	-1/3	-2/17
10	-21/2	-1/3	-2/3	-1/3	-2/17
11	-21/2	-1/3	-2/3	-1/3	-2/17
12	-21/2	-1/3	-2/3	-1/3	-2/17
13	-21/2	-1/3	-2/3	-1/3	-2/17
14	-21/2	-1/3	-2/3	-1/3	-2/17
15	-21/2	-1/3	-2/3	-1/3	-2/17
16	-21/2	-1/3	-2/3	-1/3	-2/17

$d \setminus d$	6	7	8	9	10
0	-40/3	-280/81	-218/27	-283/27	-283/27
1	-3/2	5/13	49/31	49/31	49/31
2	-8/3	-5/27	-49/27	-49/27	-49/27
3	5/23	121/531	599/519	599/519	599/519
4	-3/2	-104/567	-691/567	-691/567	-691/567
5	13/443	273/6847	329/5941	329/5941	329/5941
6	-39/7	68/6847	-17/40337	-17/40337	-17/40337
7	-1/21	33183/817	618/15243	618/15243	618/15243
8	-79/7	76/6239	-939/307	-939/307	-939/307
9	-17/2	-118/575	340/3080	340/3080	340/3080
10	-8/3	-25/27	-2/27	-2/27	-2/27
11	-1/2	-1/2	-1/2	-1/2	-1/2
12	-1/2	-1/2	-1/2	-1/2	-1/2
13	-1/2	-1/2	-1/2	-1/2	-1/2
14	-1/2	-1/2	-1/2	-1/2	-1/2
15	-1/2	-1/2	-1/2	-1/2	-1/2
16	-1/2	-1/2	-1/2	-1/2	-1/2

B.3. Local curve X_p GW invariants ($p = 3$)

$g \setminus d$	1	2	3	4	5	6	7	8	9
0	-1	-7	-39	-163	-487	-1240	-2663	-5044	-9529
1	-17	-24	-46	-102	-217	-424	-796	-1406	-2604
2	-27	-43	-77	-163	-328	-612	-1127	-2069	-3843
3	-60	-98	-178	-403	-833	-1592	-2871	-5091	-9147
4	-173	-311	-592	-1319	-2740	-5157	-9782	-18163	-33641
5	-523	-987	-1879	-4030	-8330	-15920	-28710	-50910	-91470
6	-1188	-2250	-4350	-9180	-19200	-37440	-70560	-133680	-249600
7	-3748	-7200	-13800	-28800	-57600	-111600	-212400	-401400	-756000
8	-11336	-22080	-41760	-82560	-161280	-308160	-580800	-1087200	-2030400
9	-33984	-66240	-124800	-244800	-471360	-891840	-1667040	-3117120	-5808000
10	-101760	-200640	-380160	-750720	-1452000	-2736000	-5112000	-9580800	-17872000
11	-297600	-580800	-1087200	-2124000	-4014000	-7560000	-14064000	-26040000	-48432000
12	-843840	-1612800	-3081600	-6124800	-11760000	-21240000	-40140000	-75600000	-140640000
13	-2380800	-4713600	-8918400	-17366400	-33641000	-63000000	-118176000	-220320000	-414720000
14	-6720000	-13368000	-25344000	-50140000	-95290000	-178720000	-336410000	-630000000	-1181760000
15	-18720000	-37440000	-70560000	-140640000	-273600000	-511200000	-958080000	-1787200000	-3364100000
16	-50400000	-100800000	-192000000	-380160000	-750720000	-1452000000	-2736000000	-5112000000	-9580800000
0	-1	-7	-39	-163	-487	-1240	-2663	-5044	-9529
1	-17	-24	-46	-102	-217	-424	-796	-1406	-2604
2	-27	-43	-77	-163	-328	-612	-1127	-2069	-3843
3	-60	-98	-178	-403	-833	-1592	-2871	-5091	-9147
4	-173	-311	-592	-1319	-2740	-5157	-9782	-18163	-33641
5	-523	-987	-1879	-4030	-8330	-15920	-28710	-50910	-91470
6	-1188	-2250	-4350	-9180	-19200	-37440	-70560	-133680	-249600
7	-3748	-7200	-13800	-28800	-57600	-111600	-212400	-401400	-756000
8	-11336	-22080	-41760	-82560	-161280	-308160	-580800	-1087200	-2030400
9	-33984	-66240	-124800	-244800	-471360	-891840	-1667040	-3117120	-5808000
10	-101760	-200640	-380160	-750720	-1452000	-2736000	-5112000	-9580800	-17872000
11	-297600	-580800	-1087200	-2124000	-4014000	-7560000	-14064000	-26040000	-48432000
12	-843840	-1612800	-3081600	-6124800	-11760000	-21240000	-40140000	-75600000	-140640000
13	-2380800	-4713600	-8918400	-17366400	-33641000	-63000000	-118176000	-220320000	-414720000
14	-6720000	-13368000	-25344000	-50140000	-95290000	-178720000	-336410000	-630000000	-1181760000
15	-18720000	-37440000	-70560000	-140640000	-273600000	-511200000	-958080000	-1787200000	-3364100000
16	-50400000	-100800000	-192000000	-380160000	-750720000	-1452000000	-2736000000	-5112000000	-9580800000

GW invariants ($p = 4$)

$g \setminus d$	1	2	3	4	5
0	-1	-8	-395	-655	-1351
1	$-\frac{12}{5}$	$\frac{31}{5}$	$\frac{307}{5}$	$\frac{4769}{5}$	$\frac{71829}{5}$
2	-20	-60	-333	-8671	-169307
3	-6078	-6078	10831	100857	2296569
4	-174800	-87400	27160	-4787059	-12146546
5	33740	8735	207377	60914792	6683332920
6	-11887938000	-5943974000	-69693003	-192371709171	-3501929429071663
7	5748013200	114961384	27315270	12308841839	1381179265910717
8	-71197486192000	-20927948888000	-13374909213	-11291236988439	-1214691510019390
9	3005348931232000	30654483858000	13374909213	8369115985529	434291142949429
10	-423546645780480000	-2117883322802410000	-10617831688741000	-3066883038840047	-21046943429146004617
11	5714892372762340000	5719238316969380000	8038688729132000	3066883038840047	423546645780480000
12	-7364439266673340000	-377617701444969740000	-837892469880000	-33414242345680003	-3624319238834880000
13	741836826673340000	741836826673340000	33414242345680003	33414242345680003	33414242345680003
14	-11033432847256870118323200000	-70172714236929586591616000000	-3119787299379083681849600000	-14034642847205876118232000000	-10736802190108366244864000000

$g \setminus d$	6	7	8	9
0	-2869685	61474519	1329890705	28987637150
1	18371967	464454923	113274172	136564697653
2	-5083791	-22024408093	-700464021	-7073754906361
3	2688744923	60877491271	1561613024	248490108571269
4	-5455796821	-15301192800433	-1124214980333	-5502669679238241
5	108728017888147	31299069209208831	16333699420028029	11240237269268465472726598272919
6	-6997262403293422	-7245459685277450588483	-1047802025944969348123	-2331389756866669984713991
7	265129313743877721	7245459685277450588483	11529119494005652319695509	76826764093311056746271619
8	-5178987803441793717	-242912930402944646592766531	-9976632963311709417948283407	-507588007644948012741776106611
9	9592388074938463542983	240044344023477434108670343	1820932927541339100946909443414583	11240237269268465472726598272919
10	-1847642393085829205488077	-17296441939469221723368662747363	-20422810816951695746009796686919	-1916362648390841656581957068268537
11	596414082241250107000889	368167272596124818000916	2963704723917472731480000	826318627140641284934118400
12	-60855648394839395900008731037	-78616574694884662416194006	-1359419496980000	-349444740848480000
13	124168468434664787824000	21180241627281818189400000	56749866699342499400005828117	218609764838883422662636924000
14	-10777680393383938983939	-1346923681820866011210000	-3227694110894363450000	-5679181241680823466788724000

11240237269268465472726598272919 1916362648390841656581957068268537 826318627140641284934118400 218609764838883422662636924000 10859508493487 5679181241680823466788724000 124168468434664787824000 387418383693683308194874400000 41269399107691414874400000

GW invariants ($p = 5$)

$\rho \setminus d$	1	2	3	4	5
0	-1	-31	-1081	-39711	-1502501
1	-12	82	6359	111683	1607779
2	-240	-1470	-326	-174668	-15035499Z
3	-6018	15172	20418	10725072	200334856Z
4	-172300	-332360	60418	-30625072	-85436673
5	-5322240	1330560	-7482403	1140000	315740013
6	-118848800	2977137760	-694857612765	28008382413	-273303828100261
7	-674019200	170767808	66103030829	-429498146945723	1004038082229179231
8	-7113743867	32942172800	-1500817400494581	43892814884474919029669	-2942674456881876031
9	-3005349374011	75193247780800	9044095374088863	-1770459341728980054273	6485698314818493284175687
10	-422556665784800000	1065031651865200000	-224049667470316833	690234030813191818802954	-2108449348690951357094925399
11	-6711805242672540000	167870285054188160000	265407491801088000	-241492946188067200019	25953769382347747856096872122733
12	-736443276838885319360000	16737392554527125400000	-74740276588885619260000	-2415197498089831120000033	-685669671183095257655640006
13	-7445380820958873272320000	18613120119971831680000	74458882795887327232000	26270143401433934336000043	16185610449495405924000
14	-110345428723058701182322000000	3508635711801469025858000000	-1403444287230587182322000000	-2248197232468539714423000000	44538802795887327232000084741

$\rho \setminus d$	6	7	8
0	-57240544	-2264743127	-86357415725
1	738326881	11040003661	488064205075
2	-23198531807	-1024183152753	2227984828845
3	622343282237	193386110471989	1240532237661025
4	-131134011427661	-3183366764830927	365286253160101729
5	32622313209613369	118306916500700213	105738749187611384195
6	-5188061830560	-95241870619249	889483897662879
7	121188904830048802	4402901273883270078520321	-88694143092624800
8	-622357692937388000663017	-135477122675050080827118569	569376308191831
9	783794001118336314375027311	11857688091059460402956438370103	-23685074149829709310144927033
10	-4657921614491818172116630040431	-27649288344424859459912852043137	420057663772834974264739685064039
11	880821182473077610169349048945129	7290775452056857698487231046317233	-49709827764833401089344708080217349
12	-5804834477642119016907847716516671441	-18206878800693510446584762930407929163139	707364327266864263409441911875479549571
13	1111361806077103951808114280247108546279	15006488598807004859440708274401388129219551	-4083035778902838284510245317089969810813169
14	-38421992965865711801469025858000000	-2913525863767019285145204767470000	1577126237778266623119105127750788422938137

$\rho \setminus d$	8
0	-4678180949068253277410000
1	458402109246463
2	-39321901164652721075046980605372500
3	4678180949068253277410000

$[b_{d,n}]_{X_4} \setminus n \setminus d$	3	4	5	6	7
1	30	720	15 430	318 912	6 572 342
2	12	464	11 380	255 102	5 516 812
3	6	272	8 200	200 952	4 589 830
4	0	160	5 740	156 240	3 784 480
5	0	80	3 930	119 568	3 093 020
6	0	40	2 600	90 366	2 505 328
7	0	16	1 680	67 128	2 011 576
8	0	8	1 040	49 248	1 600 592
9	0	0	630	35 472	1 262 366
10	0	0	360	25 212	986 440
11	0	0	200	17 544	763 896
12	0	0	100	12 060	585 844
13	0	0	50	8 064	445 116
14	0	0	20	5 328	334 712
15	0	0	10	3 408	249 214
16	0	0	0	2 148	183 484
17	0	0	0	1 296	133 686
18	0	0	0	780	96 180
19	0	0	0	432	68 432
20	0	0	0	240	47 992
21	0	0	0	120	33 250
22	0	0	0	60	22 652
23	0	0	0	24	15 232
24	0	0	0	12	10 024
25	0	0	0	0	6 510
26	0	0	0	0	4 116
27	0	0	0	0	2 562
28	0	0	0	0	1 540
29	0	0	0	0	910
30	0	0	0	0	504
31	0	0	0	0	280
32	0	0	0	0	140
33	0	0	0	0	70
34	0	0	0	0	28
35	0	0	0	0	14

$[b_{d,n}]_{X_5} \setminus n \setminus d$	2	3	4	5	6
1	4	-180	7 056	-260 540	9 556 212
2	0	-108	5 236	-211 520	8 175 516
3	0	-60	3 744	-169 620	6 945 208
4	0	-30	2 640	-134 270	5 856 240
5	0	-12	1 784	-104 980	4 903 560
6	0	-6	1 192	-80 980	4 075 344
7	0	0	752	-61 690	3 363 468
8	0	0	472	-46 330	2 755 086
9	0	0	272	-34 340	2 241 132
10	0	0	160	-25 060	1 808 952
11	0	0	80	-18 030	1 449 900
12	0	0	40	-12 740	1 152 810
13	0	0	16	-8 870	909 984
14	0	0	8	-6 040	712 212
15	0	0	0	-4 050	553 308
16	0	0	0	-2 640	425 880
17	0	0	0	-1 690	325 272
18	0	0	0	-1 040	245 940
19	0	0	0	-630	184 416
20	0	0	0	-360	136 728
21	0	0	0	-200	100 512
22	0	0	0	-100	72 912
23	0	0	0	-50	52 416
24	0	0	0	-20	37 116
25	0	0	0	-10	26 016
26	0	0	0	0	17 904
27	0	0	0	0	12 204
28	0	0	0	0	8 112
29	0	0	0	0	5 340
30	0	0	0	0	3 408
31	0	0	0	0	2 148
32	0	0	0	0	1 296
33	0	0	0	0	780
34	0	0	0	0	432
35	0	0	0	0	240

Large-degree expansion coefficients $\widehat{c}_{j_0}^{(j)}$

$j \setminus j_0$	1	2	3	4
1	$\frac{\sqrt{2}}{3}(f-2)$			
2	$\frac{f^2+5f+5}{18}$	$(f-2)^2$		
3	$-\frac{\sqrt{2}(f-2)(f^2+23f-23)}{810}$	$\frac{\sqrt{2}(f^2+5f-5)(f-2)}{54}$	$\frac{\sqrt{2}(f-2)^3}{81}$	
4	$-\frac{7f^4+2f^3-33f^2+62f-31}{1620}$	$\frac{7f^4-2f^3+1113f^2-2222f+1111}{9720}$	$\frac{(f-2)^2(f^2+5f-5)}{162}$	$\frac{(f-2)^4}{486}$

Free energy coefficients $a_{g,i}(p)$

i	$a_{2,i}(p)$	i	$a_{3,i}(p)$
		1	$\frac{1}{6048f^{10}}$
		2	$\frac{3f^4-70f^3+497f^2-630f+280}{241920f^{10}}$
		3	$-\frac{137f^5+1278f^4-3045f^3+3187f^2-1883f+360}{181440f^{10}}$
1	$-\frac{1}{240f^5}$	4	$\frac{1741f^6-8517f^5+17136f^4-21039f^3+13013f^2-4734f+360}{362880f^{10}}$
2	$-\frac{2f^3+25f^2+f+12}{2880f^5}$	5	$-\frac{636f^6-3031f^5+7693f^4-9638f^3+7735f^2-3031f+636}{120960f^9}$
3	$-\frac{12f^3+9f^2-35f+2}{2880f^4}$	6	$\frac{360f^6-4734f^5+13118f^4-21039f^3+17031f^2-8517f+1741}{362880f^8}$
4	$-\frac{7f+5}{2880f^2}$	7	$\frac{360f^5-1853f^4+3187f^3-3075f^2+1278f-137}{181440f^7}$
5	$\frac{f-1}{2880f}$	8	$\frac{295f^4-630f^3+482f^2-70f+3}{241920f^6}$
		9	$\frac{f^2+12f-1}{72576f^3}$
		10	$\frac{f^2-1}{725760f^2}$

If we define the following quantity (recall that $f \equiv (p-1)^2$)

$$(B.14) \quad \bar{a}_{g,i}(f) = C_g f^{6(g-1)} a_{g,i}(f) + \binom{5(g-1)}{i} (f^i - f^{i+g-1}),$$

we find that it has the following ‘‘reflection’’ property

$$(B.15) \quad \bar{a}_{g,i}(f) = f^{6(g-1)} \bar{a}_{g,5(g-1)-i} \left(\frac{1}{f} \right).$$

This would, in general, reduce the number of GW invariants needed to completely fix (4.91), from $5(g-1)$ down to $\lceil \frac{5(g-1)}{2} \rceil$. The available amount of data is unfortunately not enough to completely pinpoint a general expression for the constant C_g .

i	$a_{4,i}(p)$
1	$\frac{1}{-172800f^{15}}$
2	$\frac{2f^5 - 75f^4 + 994f^3 - 5350f^2 + 8461f - 2604}{14515200f^{15}}$
3	$-\frac{2582f^6 - 42087f^5 + 243480f^4 - 584534f^3 + 616185f^2 - 314250f + 45360}{43545600f^{15}}$
4	$\frac{88290f^7 - 910787f^6 + 3434955f^5 - 6337605f^4 + 6666425f^3 - 3968880f^2 + 1197450f - 98280}{43545600f^{15}}$
5	$-\frac{1403015f^8 - 10868010f^7 + 34735692f^6 - 63129674f^5 + 70900605f^4 - 49330860f^3 + 20133240f^2 - 3982608f + 181440}{87091200f^{15}}$
6	$\frac{3509560f^9 - 25035695f^8 + 83179010f^7 - 163178700f^6 + 202937816f^5 - 163942655f^4 + 83098100f^3 - 24287100f^2 + 3040776f - 60480}{87091200f^{15}}$
7	$-\frac{1527084f^9 + 13390590f^8 - 52041408f^7 + 115753075f^6 - 164355872f^5 + 152803338f^4 - 92842411f^3 + 34605080f^2 - 6972948f + 437688}{43545600f^{14}}$
8	$\frac{218844f^9 - 3486474f^8 + 17302540f^7 - 46417988f^6 + 76401669f^5 - 82177936f^4 + 57873320f^3 - 26020704f^2 + 6695295f - 763542}{21772800f^{13}}$
9	$-\frac{60480f^9 + 3040776f^8 - 24287100f^7 + 83108110f^6 - 163942655f^5 + 202937816f^4 - 163188710f^3 + 83179010f^2 - 25035695f + 3509560}{87091200f^{12}}$
10	$-\frac{181440f^{15} + 3982608f^{14} - 20127234f^{13} + 49330860f^{12} - 70900605f^{11} + 63123668f^{10} - 34735692f^9 + 10868010f^8 - 1403015f^7}{87091200f^{18}}$
11	$-\frac{98280f^{15} - 1198815f^{14} + 3968880f^{13} - 6666425f^{12} + 6338970f^{11} - 3434955f^{10} + 910787f^9 - 88290f^8}{43545600f^{18}}$
12	$-\frac{44905f^{15} - 314250f^{14} + 616185f^{13} - 584079f^{12} + 243480f^{11} - 42087f^{10} + 2582f^9}{43545600f^{18}}$
13	$\frac{35f^{16} - 2604f^{15} + 8461f^{14} - 5385f^{13} + 994f^{12} - 75f^{11} + 2f^{10}}{14515200f^{18}}$
14	$\frac{5f^{17} - 84f^{15} - 5f^{14}}{14515200f^{18}}$
15	$\frac{f^{18} - f^{15}}{43545600f^{18}}$

B.4. Hurwitz theory

GW invariants

$g \setminus d$	1	2	3	4	5
0	1	1	1	1	1
1	0	1	1	1	1
2	0	48	18	13	9
3	0	1440	144	70	470
4	0	80640	725760	321	1728
5	0	7257600	10884000	725760	181440
6	0	988013200	236740800	7257600	8800080
7	0	174350582400	5230678400	174350582400	153452904
8	0	4184557976000	791312000	4184557976000	10228800496
9	0	1280474711486000	3353838802400	1280474711486000	10228800496
10	0	486580001635328000	464463110651904000	486580001635328000	10228800496
11	0	2248100145555921536000	67440046069594608000	2248100145555921536000	10228800496
12	0	1241085680346617887820000	5539777193976633	1241085680346617887820000	10228800496
13	0	8065829222321271108000000	762221680222321271108000000	8065829222321271108000000	10228800496
14	0	53050571962438211727361696000000	22866625818538539376128000000	53050571962438211727361696000000	10228800496
15	0	5262616758673870633443602432000000	19271845232418240569344000000	5262616758673870633443602432000000	10228800496
16	0	50046558087920828160523721928704000000	5127073511747230595988715008000000	50046558087920828160523721928704000000	10228800496

$g \setminus d$	6	7	8	9
0	1	1	1	1
1	0	3	343	5461
2	0	10	40	4180
3	0	144	2640	20240
4	0	1440	8640	30720
5	0	15360	26208	120880
6	0	153600	275808	1208800
7	0	1536000	2758080	12088000
8	0	15360000	27580800	120880000
9	0	153600000	275808000	1208800000
10	0	1536000000	2758080000	12088000000
11	0	15360000000	27580800000	120880000000
12	0	153600000000	275808000000	1208800000000
13	0	1536000000000	2758080000000	12088000000000
14	0	15360000000000	27580800000000	120880000000000
15	0	153600000000000	275808000000000	1208800000000000
16	0	1536000000000000	2758080000000000	12088000000000000

Large-degree expansion coefficients $C_{j_0}^{H,(j)}$

$j \backslash j_0$	1	2	3	4	5	6	7
1	$\frac{\sqrt{2}}{3}$						
2	$\frac{1}{18}$	$\frac{1}{9}$					
3	$-\frac{1}{405\sqrt{2}}$	$\frac{1}{27\sqrt{2}}$	$\frac{\sqrt{2}}{81}$				
4	$-\frac{1}{1620}$	$-\frac{1}{1620}$	$\frac{1}{162}$	$\frac{1}{486}$			
5	$-\frac{1}{2268\sqrt{2}}$	$-\frac{1}{11}$	$\frac{1}{11}$	$\frac{1}{1}$	$\frac{1}{3645\sqrt{2}}$		
6	$-\frac{382725}{101}$	$-\frac{3645\sqrt{2}}{8941}$	$-\frac{14580\sqrt{2}}{29}$	$\frac{729\sqrt{2}}{37}$	$\frac{1}{8748}$	$\frac{1}{65610}$	
7	$1020600\sqrt{2}$	$-\frac{9185400}{487}$	$-\frac{58320}{11237}$	$-\frac{262440}{1}$	$\frac{1}{13}$	$\frac{1}{65610\sqrt{2}}$	$\frac{1}{688905\sqrt{2}}$

B.5. Quintic

GW invariants

$g \setminus d$	1	2	3	4	5
0			8564576000		
1	2875	4071423	2438383750	1551429277068574	22936688887648
2	2875	5125	7930325	382833353125	93716201322650
3	48	3436	106884122	10106884122	3092760574975
4	4018	2436	9916125	50440022	23896913123175
5	6012	10824	10824	4740022	4160147200
6	575	32576	404575	63287825	5200917677885
7	10478	32576	27956695575	418569469575	82282406496995
8	15848	6391458	258223348	118569469575	24388869772090845541
9	15848	38250178	118569469575	118569469575	161290779461
10	22937068	5794166568	616765411475	20510305728	211031705728
11	5600958359336	5794166568	616765411475	118569469575	66776845740618
12	210479631600876	307608897424	15026746579016	118569469575	15026746579016
13	33801529160248400	80545934208120	3439424582780	1330011801441	30078888881003
14	239538877685	80545934208120	3439424582780	1330011801441	30078888881003
15	380156221657330	211571814231960	11503643340120128720	40190107021710919	16100509144712053856541
16	26896976705008094720	9927444273181029760	48336225708348610080	271800115565153569	14518123115715180968804
17	488163020674612585472000	340238134195044848165532000	1477242959105881696666000	11007481858618241669280	70172742360948380591610000
18	91129270362443636847486668000	16724207683262216288152408000	4346130107005952322382710	278330437644829559127014000	13099833614886977430762084000
19	1508713625694924930976369745040000	13858094074240419242176894176000	12368369494968369496563696960000	336012549749568617541454760000	30249494949683694965636969444000

$g \setminus d$	6	7	8	9
0				
1	248245742157695375	101216230348800061125625	19233664640003538944306875	3657297321038982212925847031250
2	105695933333320312	80782846834330636046225	17884149295651291866599375	19766763696931421222368228125
3	45735966920745972	307920419281179807875	72245292901042275772125	200551217392534120291118125
4	86000485655933125	1644218013104575653625	965469929015339224100875	522095807026263760691031625
5	11489258585633795	14550939702782264025	54865690043329430115025	29385886046658786358654375
6	23811272612797375	1201020648040187815275	1347829233300084220975	1183218751123884844116525
7	33126322263302011	478283754671435125529275	59980780715151997732055	2903864910470846073
8	125601406381242	3018363620916054	39439744	145517952
9	1990375930170872617	2007108165869248400965	59995817294851182374085655	628173976161922912
10	940161019171272325	239934922137151544069303	13683291804242317210660821	14119958126886887249199789007
11	1536969468484545009	4204658110113279483864937	1190764930407680496545793	1131311246481110089857113995452
12	1372913569132449245	125597008662303366922	1240029236844322845913929	19637018720986930283952
13	59747816410540112	97144357846704041021120	15260593078567500	38310540243330080
14	294578110736955420744100	117832442948821684097673	7684142768498885193640	1178312442948821684097673
15	119979304530308178877	28595646569310881849001	33007420739815010904	2847801077891592569926280
16	10081291752933730181126007543	210469501717084990108286993293	13907429271503831599316811574677	232709751063558995958607451104233
17	213494470468149904887416880281	26941494980177339972516570567009011	416564829914422429634018848180753	84089939417140212249693349103500924683
18	3296633455740628482516023265197143	228574543456850401389372409928243619	3108492764502763022903835701195260689657	731461121188948714405387462274885877963
19	1731570668833932307778217574400000	1385266365808186584622227405952000	3936387884769052797222221760000	98946895363084765014446957668000

References

- [1] W. Lerche, C. Vafa, and N. P. Warner, *Chiral rings in $\mathcal{N} = 2$ superconformal theories*, Nucl. Phys. **B324** (1989), 427.
- [2] B. R. Greene and M. R. Plesser, *Duality in Calabi–Yau moduli space*, Nucl. Phys. **B338** (1990), 15.
- [3] P. Candelas, M. Lynker, and R. Schimmrigk, *Calabi–Yau manifolds in weighted \mathbb{P}^4* , Nucl. Phys. **B341** (1990) 383.
- [4] P. Candelas, X. C. De La Ossa, P. S. Green, and L. Parkes, *A pair of Calabi–Yau manifolds as an exactly soluble superconformal theory*, Nucl. Phys. **B359** (1991), 21.
- [5] E. Witten, *Phases of $\mathcal{N} = 2$ theories in two-dimensions*, Nucl. Phys. **B403** (1993), 159, [arXiv:hep-th/9301042](#).
- [6] M. Bershadsky, S. Cecotti, H. Ooguri, and C. Vafa, *Kodaira–Spencer theory of gravity and exact results for quantum string amplitudes*, Commun. Math. Phys. **165** (1994), 311, [arXiv:hep-th/9309140](#).
- [7] M. Kontsevich, *Enumeration of rational curves via torus actions*, Progr. Math. **129** (1995), 335, [arXiv:hep-th/9405035](#).
- [8] D. Ghoshal and C. Vafa, *$c = 1$ string as the topological theory of the conifold*, Nucl. Phys. **B453** (1995), 121, [arXiv:hep-th/9506122](#).
- [9] A. Strominger, S.-T. Yau, and E. Zaslow, *Mirror symmetry is T-duality*, Nucl. Phys. **B479** (1996), 243, [arXiv:hep-th/9606040](#).
- [10] K. Hori and C. Vafa, *Mirror symmetry*, [arXiv:hep-th/0002222](#).
- [11] E. Witten, *Mirror manifolds and topological field theory*, [arXiv:hep-th/9112056](#).
- [12] S. Hosono, A. Klemm, and S. Theisen, *Lectures on mirror symmetry*, Lect. Notes Phys. **436** (1994), 235, [arXiv:hep-th/9403096](#).
- [13] B. R. Greene, *String theory on Calabi–Yau manifolds*, [arXiv:hep-th/9702155](#).
- [14] M. Mariño, *Chern–Simons theory and topological strings*, Rev. Mod. Phys. **77** (2005), 675, [arXiv:hep-th/0406005](#).
- [15] M. Alim, *Lectures on mirror symmetry and topological string theory*, [arXiv:1207.0496 \[hep-th\]](#).

- [16] J. Koplik, A. Neveu, and S. Nussinov, *Some aspects of the planar perturbation series*, Nucl. Phys. **B123** (1977), 109.
- [17] G. 't Hooft, *On the convergence of planar diagram expansions*, Commun. Math. Phys. **86** (1982), 449.
- [18] D. J. Gross and V. Periwal, *String perturbation theory diverges*, Phys. Rev. Lett. **60** (1988), 2105.
- [19] J. Écalle, *Les fonctions réurgentes*, Prépub. Math. Université Paris-Sud **81-05** (1981), **81-06** (1981), **85-05** (1985).
- [20] I. Aniceto, G. Başar, and R. Schiappa, *A primer on resurgent trans-series and their asymptotics*, to appear (2016).
- [21] M. Mariño, *Open string amplitudes and large-order behavior in topological string theory*, JHEP **0803** (2008), 060, arXiv:hep-th/0612127.
- [22] M. Mariño, R. Schiappa, and M. Weiss, *Nonperturbative effects and the large-order behavior of matrix models and topological strings*, Commun. Number Theor. Phys. **2** (2008), 349, arXiv:0711.1954 [hep-th].
- [23] M. Mariño, *Nonperturbative effects and nonperturbative definitions in matrix models and topological strings*, JHEP **0812** (2008), 114, arXiv:0805.3033 [hep-th].
- [24] S. Pasquetti and R. Schiappa, *Borel and Stokes nonperturbative phenomena in topological string theory and $c = 1$ matrix models*, Ann. Henri Poincaré **11** (2010), 351, arXiv:0907.4082 [hep-th].
- [25] R. Schiappa and N. Wyllard, *An A_r threesome: Matrix models, 2d CFTs and 4d $\mathcal{N} = 2$ gauge theories*, J. Math. Phys. **51** (2010), 082304, arXiv:0911.5337 [hep-th].
- [26] A. Klemm, M. Mariño, and M. Rauch, *Direct integration and non-perturbative effects in matrix models*, JHEP **1010** (2010), 004, arXiv:1002.3846 [hep-th].
- [27] N. Drukker, M. Mariño, and P. Putrov, *Nonperturbative aspects of ABJM theory*, JHEP **1111** (2011), 141, arXiv:1103.4844 [hep-th].
- [28] I. Aniceto, R. Schiappa, and M. Vonk, *The resurgence of instantons in string theory*, Commun. Number Theor. Phys. **6** (2012), 339, arXiv:1106.5922 [hep-th].
- [29] R. Schiappa and R. Vaz, *The resurgence of instantons: Multi-cut Stokes phases and the Painlevé II equation*, Commun. Math. Phys. **330** (2014), 655, arXiv:1302.5138 [hep-th].

- [30] R. Couso-Santamaría, J. D. Edelstein, R. Schiappa, and M. Vonk, *Resurgent transseries and the holomorphic anomaly*, Ann. Henri Poincaré **17** (2016), 331, arXiv:1308.1695 [hep-th].
- [31] A. Grassi, M. Mariño, and S. Zakany, *Resumming the string perturbation series*, JHEP **1505** (2015), 038, arXiv:1405.4214 [hep-th].
- [32] R. Couso-Santamaría, J. D. Edelstein, R. Schiappa, and M. Vonk, *Resurgent transseries and the holomorphic anomaly: Nonperturbative closed strings in local \mathbb{CP}^2* , Commun. Math. Phys. **338** (2015), 285, arXiv:1407.4821 [hep-th].
- [33] I. Aniceto, J. G. Russo, and R. Schiappa, *Resurgent analysis of localizable observables in supersymmetric gauge theories*, JHEP **1503** (2015), 172, arXiv:1410.5834 [hep-th].
- [34] M. Vonk, *Resurgence and topological strings*, arXiv:1502.05711 [hep-th].
- [35] R. Couso-Santamaría, *Universality of the topological string at large radius and NS-brane resurgence*, arXiv:1507.04013 [hep-th].
- [36] M. Mariño, R. Schiappa, and M. Weiss, *Multi-instantons and multi-cuts*, J. Math. Phys. **50** (2009), 052301, arXiv:0809.2619 [hep-th].
- [37] S. Garoufalidis and M. Mariño, *Universality and asymptotics of graph counting problems in nonorientable surfaces*, arXiv:0812.1195 [math.CO].
- [38] S. Garoufalidis, A. Its, A. Kapaev, and M. Mariño, *Asymptotics of the instantons of Painlevé I*, Int. Math. Res. Notices **2012** (2012), 561, arXiv:1002.3634 [math.CA].
- [39] S. H. Katz, A. Klemm, and C. Vafa, *M-theory, topological strings and spinning black holes*, Adv. Theor. Math. Phys. **3** (1999), 1445, arXiv:hep-th/9910181.
- [40] M.-x. Huang, A. Klemm, M. Mariño, and A. Tavanfar, *Black holes and large order quantum geometry*, Phys. Rev. **D79** (2009), 066001, arXiv:0704.2440 [hep-th].
- [41] A. Klemm and E. Zaslow, *Local mirror symmetry at higher genus*, arXiv:hep-th/9906046.
- [42] Y. Konishi, *Integrality of Gopakumar–Vafa invariants of toric Calabi–Yau threefolds*, Publ. RIMS **42** (2006), 605, arXiv:math/0504188 [math.AG].

- [43] N. Caporaso, L. Griguelo, M. Mariño, S. Pasquetti, and D. Seminara, *Phase transitions, double-scaling limit, and topological strings*, Phys. Rev. **D75** (2007), 046004, [arXiv:hep-th/0606120](#).
- [44] P. Zograf, *On the large genus asymptotics of Weil–Petersson volumes*, [arXiv:0812.0544 \[math.AG\]](#).
- [45] M. Mirzakhani and P. Zograf, *Towards large genus asymptotics of intersection numbers on moduli spaces of curves*, Geom. Funct. Anal. **25** (2015), 1258, [arXiv:1112.1151 \[math.AG\]](#).
- [46] Yu. I. Manin and P. Zograf, *Invertible cohomological field theories and Weil–Petersson volumes*, Annales Inst. Fourier **50** (2000), 519, [arXiv:math/9902051 \[math.AG\]](#).
- [47] S. Garoufalidis, T. T. Q. Le, and M. Mariño, *Analyticity of the free energy of a closed 3-manifold*, SIGMA **4** (2008), 080, [arXiv:0809.2572 \[math.GT\]](#).
- [48] M. Mariño, *Les houches lectures on matrix models and topological strings*, [arXiv:hep-th/0410165](#).
- [49] R. Gopakumar and C. Vafa, *M-theory and topological strings 1*, [arXiv:hep-th/9809187](#).
- [50] R. Gopakumar and C. Vafa, *M-theory and topological strings 2*, [arXiv:hep-th/9812127](#).
- [51] H. Ooguri, Y. Oz, and Z. Yin, *D-branes on Calabi–Yau spaces and their mirrors*, Nucl. Phys. **B477** (1996), 407, [arXiv:hep-th/9606112](#).
- [52] T. Graber and E. Zaslow, *Open string Gromov–Witten invariants: Calculations and a mirror ‘theorem’*, [arXiv:hep-th/0109075](#).
- [53] P. S. Aspinwall, *D-branes on Calabi–Yau manifolds*, [arXiv:hep-th/0403166](#).
- [54] C. Faber and R. Pandharipande, *Hodge integrals and Gromov–Witten theory*, Invent. Math. **139** (2000), 173, [arXiv:math/9810173 \[math.AG\]](#).
- [55] M. Mariño and G. W. Moore, *Counting higher genus curves in a Calabi–Yau manifold*, Nucl. Phys. **B543** (1999), 592, [arXiv:hep-th/9808131](#).
- [56] T. M. Chiang, A. Klemm, S.-T. Yau, and E. Zaslow, *Local mirror symmetry: Calculations and interpretations*, Adv. Theor. Math. Phys. **3** (1999), 495, [arXiv:hep-th/9903053](#).

- [57] B. Haghighat, A. Klemm, and M. Rauch, *Integrability of the holomorphic anomaly equations*, JHEP **0810** (2008), 097, arXiv:0809.1674 [hep-th].
- [58] M. Bershadsky, S. Cecotti, H. Ooguri, and C. Vafa, *Holomorphic anomalies in topological field theories*, Nucl. Phys. **B405** (1993), 279, arXiv:hep-th/9302103.
- [59] S. Yamaguchi and S.-T. Yau, *Topological string partition functions as polynomials*, JHEP **0407** (2004), 047, arXiv:hep-th/0406078.
- [60] P. S. Aspinwall, B. R. Greene, and D. R. Morrison, *Measuring small distances in $\mathcal{N} = 2$ sigma models*, Nucl. Phys. **B420** (1994), 184, arXiv:hep-th/9311042.
- [61] O. Aharony, O. Bergman, D. L. Jafferis, and J. Maldacena, *$\mathcal{N} = 6$ superconformal Chern–Simons–Matter theories, M2-branes and their gravity duals*, JHEP **0810** (2008), 091, arXiv:0806.1218 [hep-th].
- [62] M. Mariño and P. Putrov, *Exact results in ABJM theory from topological strings*, JHEP **1006** (2010), 011, arXiv:0912.3074 [hep-th].
- [63] N. Drukker, M. Mariño, and P. Putrov, *From weak to strong coupling in ABJM theory*, Commun. Math. Phys. **306** (2011), 511, arXiv:1007.3837 [hep-th].
- [64] R. Dijkgraaf and C. Vafa, *Matrix models, topological strings, and supersymmetric gauge theories*, Nucl. Phys. **B644** (2002), 3, arXiv:hep-th/0206255.
- [65] M. Aganagic, A. Klemm, M. Mariño, and C. Vafa, *The topological vertex*, Commun. Math. Phys. **254** (2005), 425, arXiv:hep-th/0305132.
- [66] M. Alim, S.-T. Yau, and J. Zhou, *Airy equation for the topological string partition function in a scaling limit*, arXiv:1506.01375 [hep-th].
- [67] R. Pandharipande, *The Toda equations and the Gromov–Witten theory of the Riemann sphere*, Lett. Math. Phys. **53** (2000), 59, arXiv:math/9912166 [math.AG].
- [68] A. Okounkov and R. Pandharipande, *Gromov–Witten theory, Hurwitz numbers, and matrix models*, arXiv:math/0101147 [math.AG].
- [69] M.-x. Huang, A. Klemm, and S. Quackenbush, *Topological string theory on compact Calabi–Yau: Modularity and boundary conditions*, Lect. Notes Phys. **757** (2009), 45, arXiv:hep-th/0612125.

- [70] J. Bryan and R. Pandharipande, *BPS states of curves in Calabi–Yau threefolds*, *Geom. Topol.* **5** (2001), 287, [arXiv:math/0009025](#) [[math.AG](#)].

CAMGSD, DEPARTAMENTO DE MATEMÁTICA
INSTITUTO SUPERIOR TÉCNICO, UNIVERSIDADE DE LISBOA
AV. ROVISCO PAIS 1, 1049-001 LISBOA, PORTUGAL
E-mail address: santamaria@math.tecnico.ulisboa.pt

CAMGSD, DEPARTAMENTO DE MATEMÁTICA
INSTITUTO SUPERIOR TÉCNICO, UNIVERSIDADE DE LISBOA
AV. ROVISCO PAIS 1, 1049-001 LISBOA, PORTUGAL
AND DÉPARTEMENT DE PHYSIQUE THÉORIQUE & SECTION DE MATHÉMATIQUES
UNIVERSITÉ DE GENÈVE, GENÈVE, CH-1211 SWITZERLAND
E-mail address: schiappa@math.tecnico.ulisboa.pt

CAMGSD, DEPARTAMENTO DE MATEMÁTICA
INSTITUTO SUPERIOR TÉCNICO, UNIVERSIDADE DE LISBOA
AV. ROVISCO PAIS 1, 1049-001 LISBOA, PORTUGAL
AND DESY THEORY GROUP, DESY HAMBURG
NOTKESTRASSE 85, D-22603 HAMBURG, GERMANY
E-mail address: ricardo.carmo.vaz@tecnico.ulisboa.pt

RECEIVED MAY 31, 2016

ACCEPTED MARCH 17, 2017